Human Molecular Genetics, 2014, Vol. 23, No. 11 **2816–2833**
doi:10.1093/hmg/ddu099
Advance Access published on March 6, 2014

Parkinson's disease-linked human PARK9/ATP13A2 maintains zinc homeostasis and promotes α-Synuclein externalization via exosomes

Stephanie M.Y. Kong[1,†,‡], Brian K.K. Chan[1,†], Jin-Sung Park[3], Kathryn J. Hill[1], Jade B. Aitken[4,6,7], Louise Cottle[1], Hovik Farghaian[5], Adam R. Cole[5], Peter A. Lay[4], Carolyn M. Sue[3] and Antony A. Cooper[1,2,5,*]

[1]Diabetes and Obesity Program, Garvan Institute of Medical Research, Darlinghurst, New South Wales 2010, Australia, [2]St Vincent's Clinical School, Faculty of Medicine, and School of Biotechnology and Biomolecular Sciences, University of New South Wales, Sydney, New South Wales 2052, Australia, [3]Department of Neurogenetics, Kolling Institute of Medical Research, Royal North Shore Hospital and the University of Sydney, Sydney, New South Wales 2065, Australia, [4]School of Chemistry, The University of Sydney, Sydney, New South Wales 2006, Australia, [5]Neuroscience Program, Garvan Institute of Medical Research, Sydney, New South Wales 2010, Australia, [6]Australian Synchrotron, Clayton, Victoria 3168, Australia and [7]Institute of Materials Structure Science, KEK, Tsukuba, Ibaraki 305-0801, Japan

Received November 27, 2013; Revised February 2, 2014; Accepted March 3, 2014

α-Synuclein plays a central causative role in Parkinson's disease (PD). Increased expression of the P-type ATPase ion pump PARK9/ATP13A2 suppresses α-Synuclein toxicity in primary neurons. Our data indicate that ATP13A2 encodes a zinc pump; neurospheres from a compound heterozygous ATP13A2$^{-/-}$ patient and ATP13A2 knockdown cells are sensitive to zinc, whereas ATP13A2 over-expression in primary neurons confers zinc resistance. Reduced ATP13A2 expression significantly decreased vesicular zinc levels, indicating ATP13A2 facilitates transport of zinc into membrane-bound compartments or vesicles. Endogenous ATP13A2 localized to multi-vesicular bodies (MVBs), a late endosomal compartment located at the convergence point of the endosomal and autophagic pathways. Dysfunction in MVBs can cause a range of detrimental effects including lysosomal dysfunction and impaired delivery of endocytosed proteins/autophagy cargo to the lysosome, both of which have been observed in cells with reduced ATP13A2 function. MVBs also serve as the source of intra-luminal nanovesicles released extracellularly as exosomes that can contain a range of cargoes including α-Synuclein. Elevated ATP13A2 expression reduced intracellular α-Synuclein levels and increased α-Synuclein externalization in exosomes >3-fold whereas ATP13A2 knockdown decreased α-Synuclein externalization. An increased export of exosome-associated α-Synuclein may explain why surviving neurons of the substantia nigra pars compacta in sporadic PD patients were observed to over-express ATP13A2. We propose ATP13A2's modulation of zinc levels in MVBs can regulate the biogenesis of exosomes capable of containing α-Synuclein. Our data indicate that ATP13A2 is the first PD-associated gene involved in exosome biogenesis and indicates a potential neuroprotective role of exosomes in PD.

*To whom correspondence should be addressed at: Diabetes and Obesity Program, Garvan Institute of Medical Research, Darlinghurst, New South Wales 2010, Australia. Email: a.cooper@garvan.org.au
†These authors contributed equally to this work.
‡Present address: Victor Chang Cardiac Research Institute, Sydney, New South Wales, 2010, Australia.

© *The Author 2014. Published by Oxford University Press. All rights reserved.*
For Permissions, please email: journals.permissions@oup.com

Downloaded from http://hmg.oxfordjournals.org/ at University of New South Wales on October 13, 2014

INTRODUCTION

Parkinson's disease (PD) is a progressive age-related movement disorder that results primarily from the selective loss of midbrain dopaminergic (DA) neurons while more widespread pathology can occur, especially at later stages of the disease (1). Although the molecular mechanisms underlying PD are unknown, considerable evidence supports the involvement of the cytosolic protein α-Synuclein in a central causative role. α-Synuclein is a predominant component deposited in Lewy Bodies, the pathological hallmark of PD (2). Allele duplication or triplication of the wild-type α-Synuclein gene (*SNCA*) results in autosomal dominant PD with a severity proportional to the degree of α-Synuclein over-expression (3) whereas missense mutations in *SNCA* (e.g. A53T) are linked to dominantly inherited forms of PD (4). Most significantly, genome-wide association studies in multiple populations found that sporadic PD, which comprises 80–90% of patients, has a very significant association with the *SNCA* locus (5,6).

Modified or elevated expression of α-Synuclein can act in a toxic manner, and thus reducing intra-neural α-Synuclein levels or suppressing its negative effects is an important therapeutic endeavour. Approaches undertaken to suppress the toxic effects of α-Synuclein include: impairing the degeneration-associated phosphorylation of α-Synuclein, si/shRNA-mediated knockdown of α-Synuclein expression or enhanced autophagy as a mechanism to decrease α-Synuclein levels (7,8). An unbiased screen in an α-Synuclein-based PD model system identified over-expression of the yeast gene *YPK9* as a suppressor of α-Synuclein-induced toxicity (9). *YPK9* is an orthologue of human *ATP13A2*, and the over-expression of *ATP13A2* was subsequently shown to rescue α-Synuclein-induced neurodegeneration in multiple models, including rat midbrain primary DA neurons (9).

ATP13A2 was identified as encoding a predicted polytopic P-type ATPase transporter of unknown ion specificity (10) which, when mutated, resulted in early onset Kufor–Rakeb syndrome, an autosomal recessive juvenile onset form of L-DOPA-responsive parkinsonism that exhibits clinical features of PD (11,12). ATP13A2 is highly expressed in the human brain with highest expression in the substantia nigra pars compacta (SNc), a region that displays progressive DA neurodegeneration in PD (12). Furthermore, surviving DA neurons in the SNc of sporadic PD patients expressed ATP13A2 mRNA at 5- to 10-fold higher levels than controls (12) whereas ATP13A2 protein levels were also found to be increased in surviving SNc neurons of PD patients relative to controls (13). This is an intriguing observation given that ATP13A2 over-expression in primary DA neurons suppresses α-Synuclein toxicity (9) and raises the possibility that elevated ATP13A2 expression may contribute to the survival of the SNc neurons in sporadic PD. Identifying ATP13A2's function could provide potential therapeutic approaches to enhance neuronal survival and ameliorate the neural degeneration underlying PD.

ATP13A2 and its yeast orthologue *YPK9* are members of the P_5 subfamily of ATPases, which utilize ATP to pump inorganic cations such as metal ions (10). To identify the metal ions likely to be transported by ATP13A2, yeast cells lacking *YPK9* (*ypk9*Δ) were challenged with different metal ions and showed an increased sensitivity to manganese relative to control cells (9), suggesting that *YPK9* and its orthologue ATP13A2 might transport manganese. However, neither ATP13A2$^{-/-}$ patient cells nor human cells with reduced ATP13A2 expression have yet to be tested for sensitivity to manganese or to any other metal.

The localization of epitope-tagged ATP13A2 to lysosomes (12–15) resulted in an examination of lysosomal dysfunction in cells with reduced ATP13A2 expression where decreased lysosomal proteolysis (14,15), impaired mitochondrial function (13,16) and decreased autophagic flux were observed. Autophagy, specifically macroautophagy, is a lysosomal degradation process that removes damaged and long-lived proteins, protein aggregates, and damaged organelles such as mitochondria (17,18). By serving to prevent accumulation of toxic material within the cell, it plays a critical neuroprotective role, as evidenced by its inactivation resulting in extensive neurodegeneration (19). The hallmark of autophagy is the sequestration of cytoplasm into a LC3-labelled double-membrane vesicle termed an autophagosome, which then fuses with degradative compartments in the endosomal/lysosomal pathway to result in the degradation of the inner vesicle and its contents (20). Perturbed lysosomal function and/or impaired autophagy in ATP13A2-deficient cells may contribute to the neurodegeneration of ATP13A2$^{-/-}$ patients as autophagy can deliver α-Synuclein to lysosomes for degradation (21). Conversely, the suppression of α-Synuclein toxicity by increased ATP13A2 expression (9) might be mediated by enhanced lysosomal delivery of α-Synuclein.

Here we show that endogenous human ATP13A2 contributes to zinc homeostasis, most likely by acting as a zinc transporter, and is found in the multi-vesicular body (MVB), a late endosomal compartment that represents a dynamic and important convergence point of the endosomal and autophagic pathways prior to lysosomal delivery. Alternatively MVBs can fuse with the plasma membrane to release extracellular vesicles termed exosomes that have the potential of intercellular transfer and have recently been implicated in a number of neurodegenerative diseases (22). We report that elevated ATP13A2 expression reduces intracellular α-Synuclein levels via increased externalization of exosome-associated α-Synuclein whereas reduced ATP13A2 expression resulted in decreased levels of exosomal α-Synuclein.

RESULTS

Yeast ATP13A2 (*YPK9*) expression levels alter zinc and manganese homeostasis

In an expanded examination of metal ion sensitivity, we found that yeast cells lacking the ATP13A2 orthologue *YPK9* (*ypk9*Δ) displayed sensitivity to manganese (ionic form Mn^{2+}) (Fig. 1), as had been observed previously (9), but displayed greater sensitivity to zinc (ionic form Zn^{2+}). Conversely, *YPK9* over-expression in wild-type yeast cells conferred resistance to both Mn^{2+} and Zn^{2+} (Fig. 1). Together these data suggest that Ypk9, and potentially human ATP13A2, encodes an ATP-driven pump capable of transporting Zn^{2+} and Mn^{2+}. *ypk9*Δ cells were also tested for sensitivity to the transition metals cobalt and iron, but no significant sensitivity was detected for these two metals (data not shown).

Downloaded from http://hmg.oxfordjournals.org/ at University of New South Wales on October 13, 2014

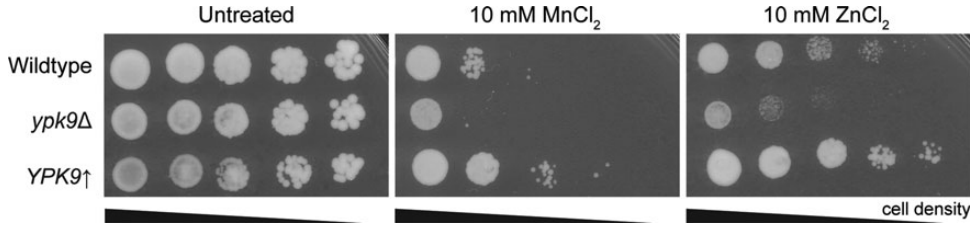

Figure 1. Zinc tolerance is dependent on *YPK9* expression levels. Wild-type, *ypk9*Δ and wild-type cells over-expressing *YPK9* (*YPK9*↑) were grown, serially diluted and spotted onto media with or without manganese or zinc. Differential sensitivity is determined by the growth difference in spot numbers between the wild-type cells and either the *ypk9Δ* cells or *YPK9* over-expressing cells, not the total number of spots that grow.

Reduced human ATP13A2 expression results in zinc but not manganese sensitivity

To determine whether reduced ATP13A2 expression in human cells increased sensitivity to Zn^{2+} and/or Mn^{2+}, we knocked down ATP13A2 expression in the human DA neuroblastoma SHSY5Y cell line that can be efficiently differentiated to neuron-like cells. To confirm ATP13A2 knockdown, we generated anti-ATP13A2 polyclonal antibodies that were capable of detecting endogenous levels of ATP13A2 protein. Immunoblotting found that these affinity-purified antibodies recognized endogenous levels of ATP13A2 in SHSY5Y cells as evidenced by a single band at the predicted molecular mass (128 kDa) that co-migrated (Supplementary Material, Fig. S1A) with V5 epitope-tagged ATP13A2 (12). SHSY5Y cells transfected with a pool of four human ATP13A2 siRNAs displayed significantly lowered ATP13A2 protein expression relative to control cells transfected with non-targeting siRNA (Supplementary Material, Fig. S1B), demonstrating both successful ATP13A2 knockdown and antibody specificity. The most effective ATP13A2 siRNA was used to generate a lentiviral shRNA plasmid to create a stable ATP13A2 knockdown SHSY5Y cell line (shPK9). Reduced ATP13A2 expression in these cells was confirmed by immunoblot (Supplementary Material, Fig. S1C) where ATP13A2 protein expression levels were reduced by ~80% (Supplementary Material, Fig. S1D).

Differentiated shPK9 cells treated with 125 μM Zn^{2+} suffered a 1.9-fold reduction in viability ($P < 0.001$) with respect to control cells (Fig. 2A) yet displayed no increased sensitivity to Mn^{2+} (Fig. 2B). These data demonstrate that, in contrast to the loss of yeast *YPK9* (*ypk9*Δ), reduced human ATP13A2 expression sensitizes neuron-like cells to Zn^{2+} but not to Mn^{2+}, supporting a role for ATP13A2 in Zn^{2+} homeostasis.

ATP13A2$^{-/-}$ patient human olfactory neurospheres are sensitive to zinc but not to manganese

To further investigate ATP13A2's role in Zn^{2+} homeostasis, human olfactory neurospheres (hONs) from an ATP13A2 compound heterozygous patient (designated ATP13A2$^{-/-}$; (11)) were generated and the extracted proteins immunoblotted. Endogenous ATP13A2 was readily detectable in control hONs but not in ATP13A2$^{-/-}$ patient extracts (Fig. 2C). ATP13A2$^{-/-}$ patient and control hONs were then tested for sensitivity to Zn^{2+} and Mn^{2+} using a viability assay. ATP13A2$^{-/-}$ patient hONs were 10-fold more sensitive to 125 μM Zn^{2+} than control cells ($P < 0.0001$) (Fig. 2D) but interestingly displayed no increased sensitivity to 5000 μM Mn^{2+} relative to control cells (Fig. 2E). Our data from human ATP13A2$^{-/-}$ patients further support the model that ATP13A2 plays a role in Zn^{2+} homeostasis.

ATP13A2$^{-/-}$ patient hONs accumulate zinc

Further evidence of zinc dyshomeostasis in ATP13A2$^{-/-}$ patient hONs was sought through the use of synchrotron X-ray fluorescence microscopy (μ-XRF), which examines total intracellular element content (23). ATP13A2$^{-/-}$ patient hONs had very similar Zn^{2+} and Mn^{2+} levels to those of control hONs (Fig. 2F). However, when challenged with 100 μM Zn^{2+}, ATP13A2$^{-/-}$ patient hONs displayed a 60% increase in total intracellular Zn^{2+} content ($P < 0.05$) compared with control hONs (Fig. 2F), suggesting that ATP13A2 may contribute to Zn^{2+} efflux from the cell. Consistent with the lack of sensitivity to Mn^{2+} (Fig. 2E), treatment of ATP13A2$^{-/-}$ patient hONs with 1 mM Mn^{2+} did not result in increased manganese accumulation relative to controls (Fig. 2G).

Elevated ATP13A2 expression in rat primary cortical neurons confers zinc resistance

To determine whether elevated ATP13A2 expression conferred Zn^{2+} resistance, control and ATP13A2 over-expressing rat primary cortical neurons (Fig. 3A) were challenged with Zn^{2+}. Morphological assessment using reduced neurite length as an indicator of neurotoxicity (24,25) found that treatment of control neurons with 180 μM Zn^{2+} caused the retraction of neurites to an average length of 18 μm (Fig. 3B and D). In contrast, elevated ATP13A2 expression conferred Zn^{2+} resistance as indicated by the neurites preserved to an average length of 96 μm ($P < 0.05$) (Fig. 3C and D) and a 2.4-fold increase in cell viability (Fig. 3E) ($P < 0.01$).

Association of endogenous ATP13A2 with autophagosomes and MVBs

Identifying the subcellular localization of ATP13A2 would provide critical clues as to how ATP13A2 impacts Zn^{2+} homeostasis and assist in understanding how elevated ATP13A2 expression suppresses α-Synuclein toxicity. We created a SHSY5Y cell line that stably expressed ATP13A2-V5–6xHis (12) and staining with V5 antibody localized ATP13A2-V5–6xHis to lysosomes as indicated by co-localization with the lysosomal marker proteins LAMP1 and LAMP2 (Fig. 4A).

Although consistent with the lysosomal localization observed by several groups using transfected ATP13A2-V5–6xHis or ATP13A2-GFP (12–15), a caveat remained that either

Downloaded from http://hmg.oxfordjournals.org/ at University of New South Wales on October 13, 2014

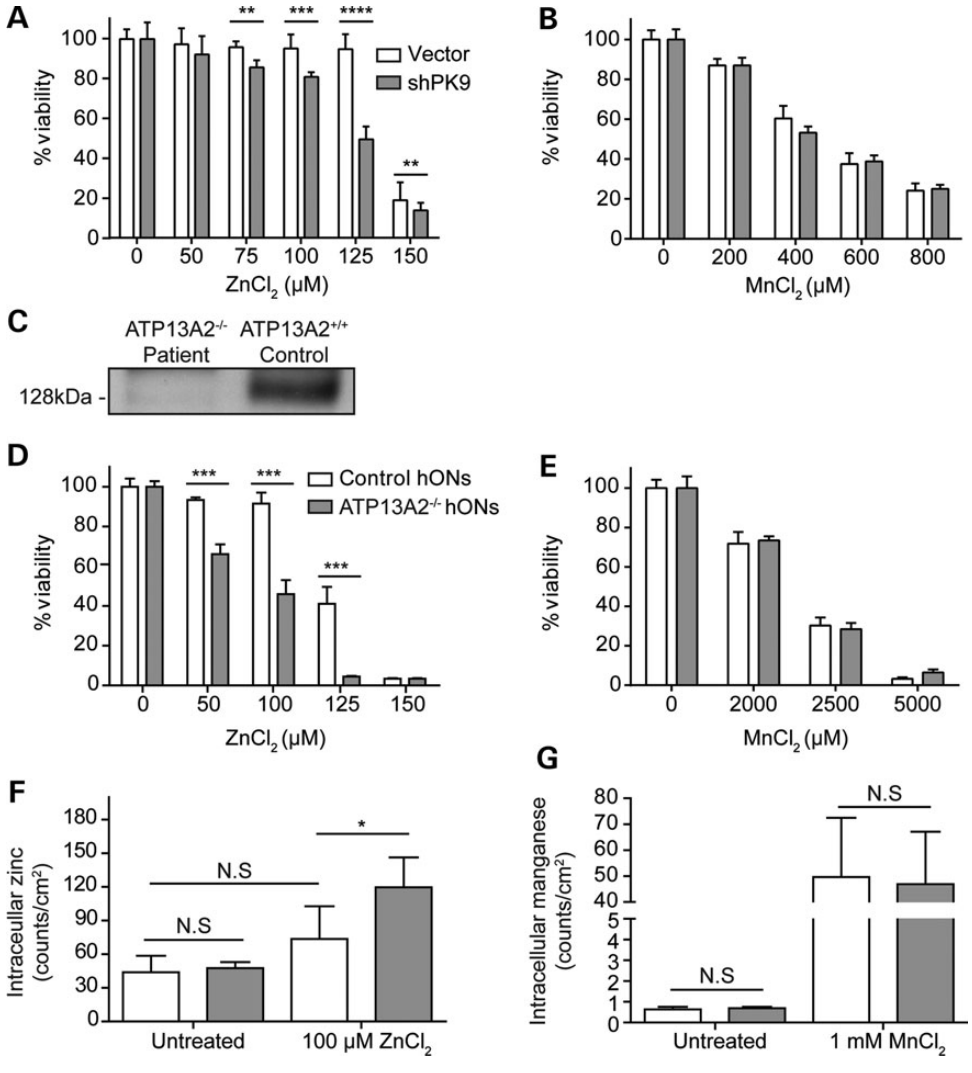

Figure 2. Reduced ATP13A2 expression confers zinc sensitivity in SHSY5Y cells and human patient cells. SHSY5Y cells stably infected with either vector or PARK9 shRNA (shPK9) encoding lentivirus were differentiated and treated with zinc (**A**) or manganese (**B**) at concentrations indicated and viability assayed. Data are from six biological replicates ($^{*}P < 0.05$, $^{**}P < 0.001$). Statistical analysis was conducted by a Student's *t*-test. (**C**) Immunoblots of proteins extracted from ATP13A2$^{-/-}$ patient and control (ATP13A2$^{+/+}$) hONs were probed with anti-ATP13A2 antibody. Control and ATP13A2$^{-/-}$ patient hONs were treated with zinc (**D**) or manganese (**E**) at concentrations indicated and cell viability assayed ($^{***}P < 0.0001$). Statistical analysis was conducted by a Student's *t*-test. Control and ATP13A2$^{-/-}$ patient hONs were cultured with either 100 μM zinc (**F**), or 1 mM manganese (**G**), and intracellular zinc/manganese quantified by measuring elemental content in cellular ROI's from μ-XRF images ($^{*}P < 0.05$). Statistical analysis was conducted by one-way ANOVA with Bonferroni *post-hoc* analysis. Data are represented as mean ± SD.

over-expression via the CMV promoter and/or epitope tagging might have caused mislocalization of ATP13A2-V5–6xHis to lysosomes, a possibility raised by Ramirez *et al*. (12).

In contrast to ATP13A2-V5–6xHis, endogenous ATP13A2 in differentiated SHSY5Y cells displayed a punctate, vesicular pattern that was clearly distinct, both in subcellular distribution and morphology, from the lysosomal proteins LAMP1 and LAMP2 (Fig. 4B). These data suggest that ATP13A2 exists on non-lysosomal vesicular structures into which it may facilitate the transport of Zn^{2+}. High concentrations of Zn^{2+} in vesicles/organelles (referred to as vesicular zinc) have been observed previously using zinquin, a lipophillic Zn^{2+}-specific fluorescent probe with affinity for vesicular zinc (26,27). If ATP13A2 facilitates transport of Zn^{2+} into such vesicles, then a reduction in ATP13A2 expression should reduce vesicular Zn^{2+} concentration and zinquin staining. We observed a characteristic multi-puncta zinquin staining pattern in differentiated SHSY5Y cells (Fig. 4C), whereas zinquin staining in differentiated shPK9 cells showed a >50% decrease ($P < 0.0001$) (Fig. 4C and D), indicating that the transport of Zn^{2+} into these vesicular structures is dependent upon ATP13A2. A large decrease in zinquin staining ($P < 0.0001$) was also observed in HEK293 cells that were knocked down for ATP13A2 expression (Fig. 4E).

The function of ATP13A2 and the consequences of its dysfunction would be aided by identifying its subcellular localization. Endogenous ATP13A2 did not significantly co-localize with markers of the endoplasmic reticulum (Calnexin), *cis*-Golgi (GM130), *trans*-Golgi (p230), early endosomes (EEA1, Rab5-GFP) or late endosomes (Rab7-GFP) by indirect immunofluorescence (Supplementary Material, Fig. S2). However, a close

Downloaded from http://hmg.oxfordjournals.org/ at University of New South Wales on October 13, 2014

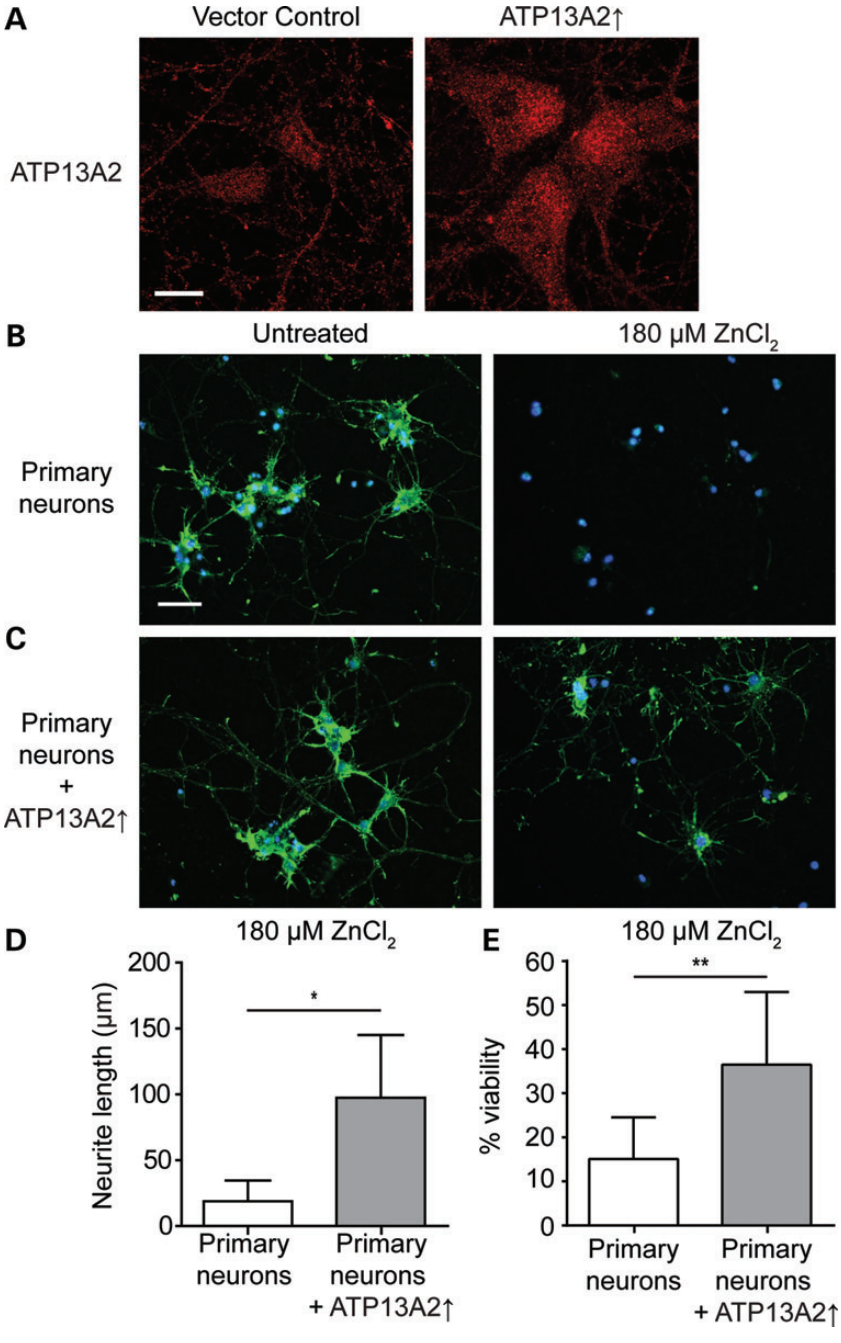

Figure 3. ATP13A2 over-expression confers zinc resistance in primary neurons. (**A**) Rat primary neurons infected with vector or ATP13A2 over-expressing lentivirus and stained with anti-ATP13A2 antibody. Scale bar = 10 μm. Control rat primary neurons have decreased viability with 180 μM zinc treatment (**B**), whereas rat neurons infected with ATP13A2 over-expressing lentivirus (**C**) are resistant to 180 μM zinc treatment. Rat primary neurons were cultured and exposed to zinc for 48 h before fixing and staining with phalloidin (green) and DAPI (blue). Scale bar = 25 μm. (**D**) Analysis of neurite length in rat primary neurons with and without over-expression of ATP3A2 after treatment of 180 μM zinc. Analysis conducted using Simple Neurite Tracer, Fiji ($^{*}P < 0.05$). Statistical analysis was conducted by one-way ANOVA with Bonferroni *post-hoc* analysis. (**E**) Analysis of live neurons by nuclear counting of dead neurons (stained with ethidium homodimer) compared with total neurons (stained with DAPI) in rat primary neuron with and without ATP13A2 over-expression after treatment of 180 μM zinc ($^{**}P < 0.01$). Statistical analysis was conducted by a Student's *t*-test. Data are represented as mean ± SD.

association was apparent between endogenous ATP13A2 and LC3, a marker of autophagosomes, in both differentiated SHSY5Y cells (Fig. 5A) and rat primary neurons (Fig. 5B).

Lysosomal delivery of autophagosomes was pharmacologically inhibited to stabilize and enhance the detection of the ATP13A2-LC3 association. Cells were treated with chloroquine (CQ), an effective inhibitor of the later stage(s) of autophagy, that is thought to act by neutralizing acidic endo-lysosomal compartments and impairing fusion of autophagosomes with these compartments (17). Treatment of differentiated SHSY5Y cells with CQ resulted in a dramatic redistribution of endogenous ATP13A2, such that it surrounded LC3-labelled autophagosomes (Fig. 5C). This association

Downloaded from http://hmg.oxfordjournals.org/ at University of New South Wales on October 13, 2014

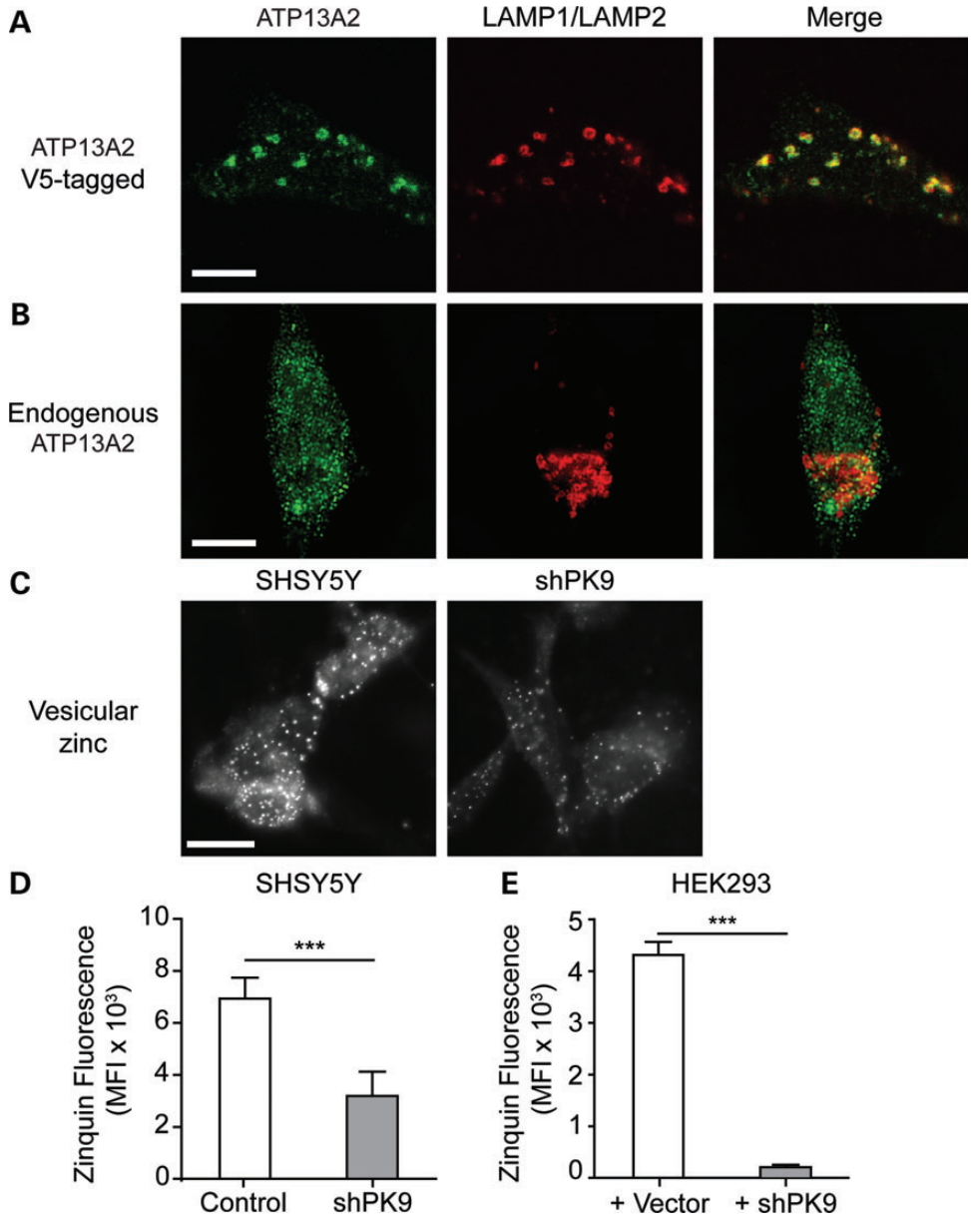

Figure 4. Endogenous ATP13A2 localizes to vesicular structures that contain zinc. (**A**) ATP13A2-V5-6xHis localized to lysosomes as indicated by co-localization with lysosomal markers, LAMP1 and LAMP2. (**B**) Endogenous ATP13A2 displayed a vesicular, punctate signal with an absence of co-localization with LAMP1 and LAMP2. (**C**) Reduced expression of ATP13A2 in SHSY5Y cells decreases zinquin fluorescence. Zinquin FACS analysis on SHSY5Y vector control and SHSY5Y-shPK9 cells (**D**) and HEK293 cells were transfected with vector or the ATP13A2 knockdown plasmid (**E**). Cells were stained with zinquin, the zinquin fluorescence quantified by FACS analysis and gated for GFP (a marker for shPK9) (*** $P < 0.0001$). Statistical analysis conducted by a Student's *t*-test. Image B was captured on a Nikon N-SIM Super Resolution Microscope. Scale bar = 10 μm.

did not represent an autophagosome fused with the lysosome (autophagolysosome) as the ATP13A2-LC3-positive structures were devoid of LAMP1 staining (Fig. 5D). A close association of endogenous ATP13A2 with LC3 is significant as impaired autophagy is closely linked with neurodegeneration and autophagosomes have been found to contain Zn^{2+} (28).

Elevated ATP13A2 expression reduces intracellular α-Synuclein protein levels

A role for ATP13A2 in autophagy may account for the observed suppression of α-Synuclein toxicity by ATP13A2 overexpression (9) as elevated ATP13A2 levels might enhance autophagic rates and result in decreased levels of α-Synuclein. To test this, a well-characterized SHSY5Y stable cell line that conditionally expresses α-Synuclein [SHSY5Y-αSyn (29)] was infected with lentivirus-encoding untagged ATP13A2 (9). The resulting stable cells (SHSY5Y-αSyn-PK9) and control SHSY5Y-αSyn cells were differentiated, α-Synuclein expression induced and α-Synuclein levels determined by immunoblot. SHSY5Y-αSyn-PK9 cells contained 60% less intracellular α-Synuclein than SHSY5Y-αSyn cells ($P < 0.001$) (Fig. 6A), consistent with increased autophagic delivery of α-Synuclein to the lysosome for degradation.

Downloaded from http://hmg.oxfordjournals.org/ at University of New South Wales on October 13, 2014

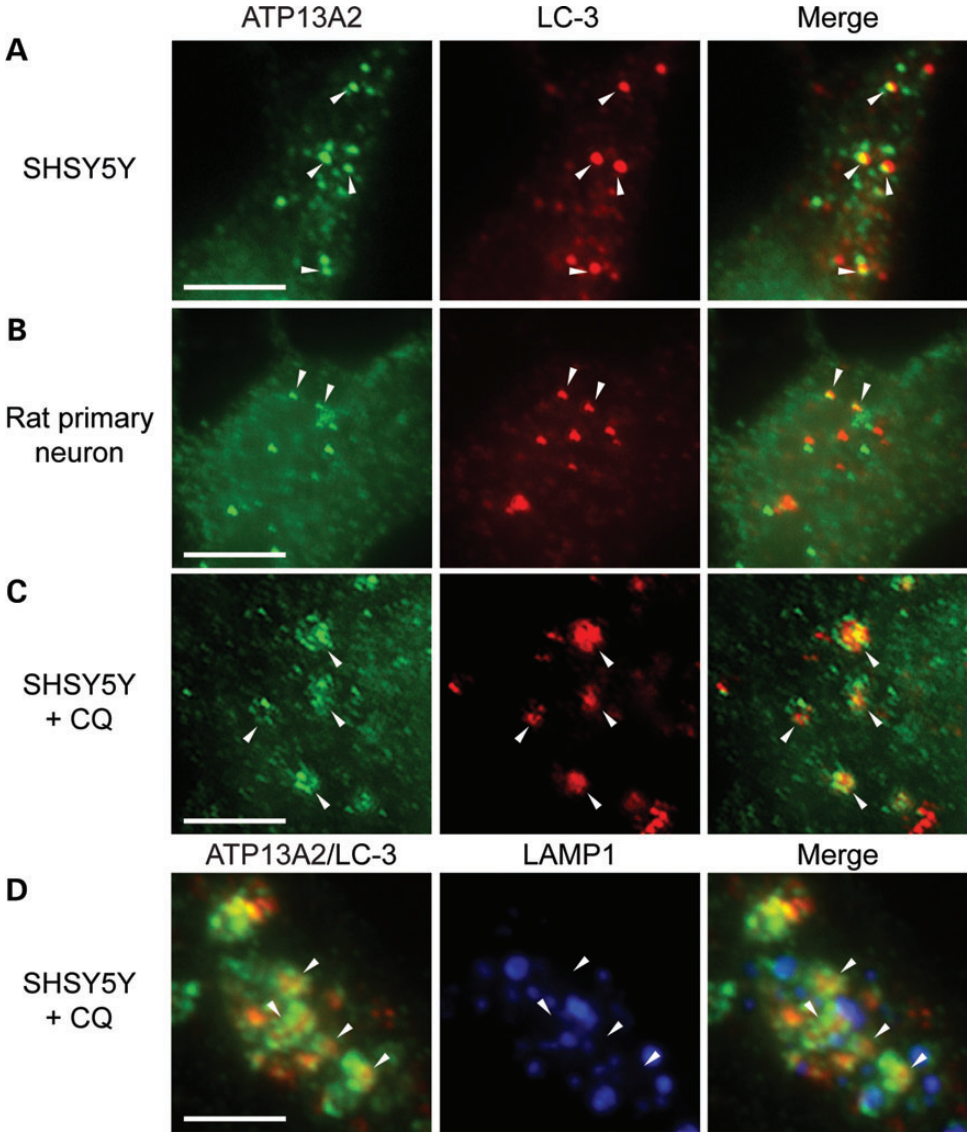

Figure 5. Endogenous ATP13A2 associates with autophagosomes not associated with lysosomes. Endogenous ATP13A2 is closely associated with endogenous LC3 puncta in differentiated SHSY5Y cells (**A**) and rat primary neurons (**B**) as indicated by arrowheads. (**C**) CQ treatment of SHSY5Y cells resulted in a redistribution of endogenous ATP13A2 into rings surrounding LC3-positive autophagosomes as indicated by arrowheads. (**D**) Triple-staining of CQ-treated SHSY5Y cells shows ATP13A2 rings (green) surrounding LC-3-postive autophagosomes (red) that have not fused with lysosomes, as indicative by the lack of overlap with LAMP1 (blue). Arrowheads indicate co-localization of ATP13A2 and LC-3 and an absence of LAMP1 staining. Scale bar = 5 μm.

Evidence of lysosomal degradation can be demonstrated using CQ to impair lysosomal delivery and proteolysis, thus allowing increased detection of a now stabilized lysosomal substrate (30). Surprisingly, CQ did not stabilize intracellular α-Synuclein levels in SHSY5Y-αSyn-PK9 cells compared with those of SHSY5Y-αSyn cells (Fig. 6B). CQ treatment successfully impaired lysosomal degradative function as evidenced by increased levels of autophagosome-associated LC3-II (Supplementary Material, Fig. S3B), which is normally rapidly degraded upon delivery to lysosomes (31). Furthermore, LC3-II levels in CQ-treated cells were not increased upon ATP13A2 over-expression (Supplementary Material, Fig. S3A), indicating that the reduction of α-Synuclein levels by ATP13A2 was not through enhanced activation of autophagy. Together these data indicate that the reduced level of intracellular α-Synuclein observed with ATP13A2 over-expression was not due to increased delivery to the lysosome. qRT-PCR analysis found that the decreased intracellular α-Synuclein protein levels associated with elevated ATP13A2 levels was not due to decreased α-Synuclein mRNA levels (Supplementary Material, Fig. S3C).

Externalization of α-Synuclein in exosomes by ATP13A2

ATP13A2′s association with autophagosomes in the absence of lysosomal delivery (Fig. 5D) prompted us to examine MVBs, which have been shown to fuse with autophagosomes to produce hybrid structures referred to as amphisomes (32). MVBs are dynamic late endosomes that participate in numerous endocytic and trafficking functions including rapid and complex protein and lipid sorting via inward budding of the MVB outer

Downloaded from http://hmg.oxfordjournals.org/ at University of New South Wales on October 13, 2014

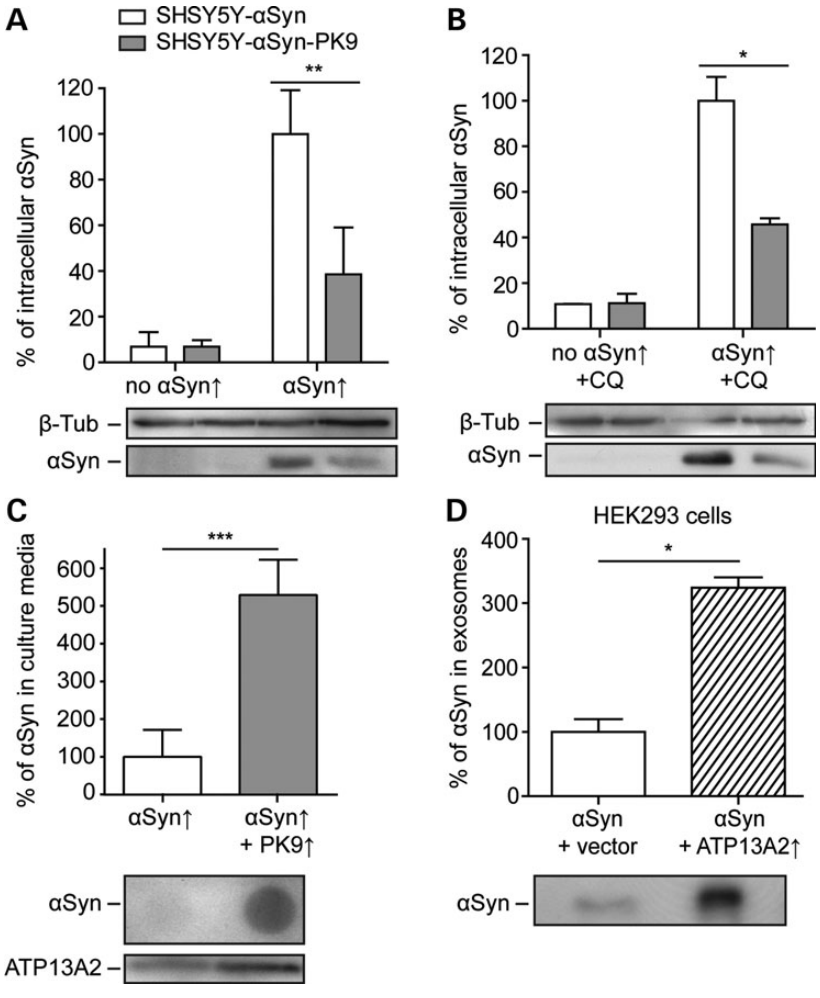

Figure 6. ATP13A2 over-expression reduces intracellular and increases extracellular α-Synuclein (αSyn) levels. Protein extracts from SHSY5Y-αSyn and SHSY5Y-αSyn-PK9 cells, un-induced (no αSyn↑) or induced for elevated human wild-type αSyn expression (αSyn↑) without (**A**) and with CQ treatment (**B**) were immunoblotted and probed with anti-α-Synuclein antibody. Data are representative of three replicates. Levels of α-Synuclein over-expression in SHSY5Y-αSyn cells were set to 100% for each replicate ($^{*}P < 0.05$, $^{**}P < 0.001$). Statistical analysis conducted by one-way ANOVA with Bonferroni *post-hoc* analysis. Cell-free culture media of SHSY5Y-αSyn and SHSY5Y-αSyn-PK9 cells (**C**), and purified exosomes from HEK293 cells (**D**) were immunobloted and probed with anti-α-Synuclein antibody. Data are representative of three replicates. Statistical analysis conducted by a Student's *t*-test. ($^{*}P < 0.05$). Data are represented as mean ± SD.

limiting membrane into the lumen to produce multiple intraluminal vesicles (ILVs) (33).

Using CQ to preserve these dynamic structures, ATP13A2 displayed extensive association with LBPA (lysobisphosphatidic acid, also termed BMP, Fig. 7A), a lipid highly enriched in ILVs (34,35). ATP13A2 staining was also seen to encircle CD63 (Fig. 7B), a tetraspanin protein also highly enriched in ILVs (36). Triple labelling allowed the detection of ATP13A2 in the same compartment with both LC3 and CD63 (Fig. 7C), strongly suggesting that membrane spanning ATP13A2 occupies the outer limiting membrane of MVBs and amphisomes.

Our data show that elevated ATP13A2 lowers intracellular α-Synuclein levels and that ATP13A2 can associate with autophagosomes and MVBs. Although both autophagosomes and MVBs can fuse with lysosomes for degradation, we found that lysosomal inhibition failed to stabilize ATP13A2-dependent lowering of α-Synuclein levels (Fig. 6B), suggesting lysosomal delivery/degradation is not involved. However, MVBs can also fuse with the plasma membrane and release ILVs extracellularly as exosomes (33). Given that SHSY5Y-αSyn cells have previously been shown to produce α-Synuclein-containing exosomes (37), ATP13A2, in associating with MVBs, might influence the generation of α-Synuclein-containing ILVs and/or the release of ILVs from the cell as exosomes.

To determine whether over-expression of ATP13A2 enhanced externalization of α-Synuclein, cell-free culture medium from SHSY5Y-αSyn and SHSY5Y-αSyn-PK9 cells was concentrated on nitrocellulose membranes and probed with anti-α-Synuclein antibodies. Confirming previous studies (37), immunoblots detected α-Synuclein in the culture medium from SHSY5Y-αSyn cells; however, ~5-fold more α-Synuclein was detected in culture medium from SHSY5Y-αSyn-PK9 cells (Fig. 6C) ($P < 0.0001$), indicating that elevated ATP13A2 expression may lower α-Synuclein levels within these cells by externalizing α-Synuclein in exosomes. To further investigate this potential ATP13A2–exosome relationship, we employed HEK293 cells as they have

Downloaded from http://hmg.oxfordjournals.org/ at University of New South Wales on October 13, 2014

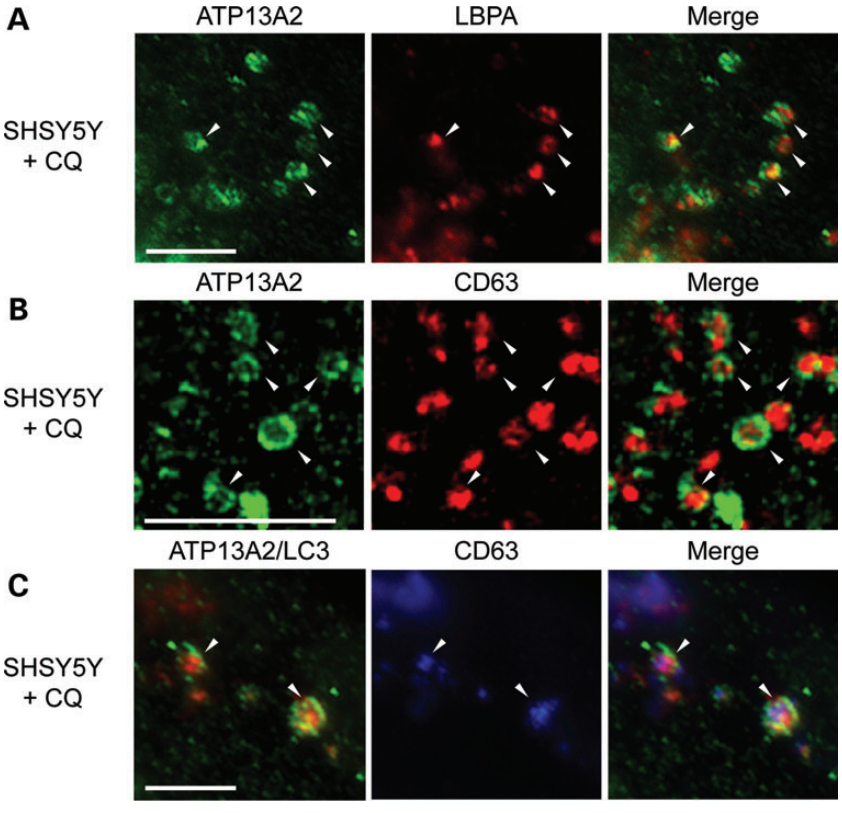

Figure 7. Endogenous ATP13A2 associates with MVBs fused with autophagosomes, which form amphisomes. In CQ-treated SHSY5Y cells, endogenous ATP13A2 'rings' surround LBPA-positive MVBs (**A**) and CD63-positive MVBs (**B**) as indicated by arrowheads. ATP13A2 is also localized to CD63-positive MVBs fused with LC3-positive autophagosomes (**C**) as indicated by arrowheads. Image B was captured on a Nikon N-SIM Super Resolution Microscope. Scale bar = 5 μm.

been used extensively to characterize exosomes owing to their high yield capacity (38,39). HEK293 cells were co-transfected with a plasmid expressing human wild-type α-Synuclein and either a vector control or plasmid expressing untagged ATP13A2. Exosomes were then purified from cell-free culture media via ultracentrifugation and the resulting immunoblots successfully probed against five different exosomal markers [Alix, CD63, Flotillin, Hsp70 and Tsg101 (40), Supplementary Material, Fig. S4], which demonstrated successful exosome purification. Elevated ATP13A2 expression resulted in a 3-fold increase ($P < 0.05$) in the amount of α-Synuclein associated with exosomes (Fig. 6D). The exosome fractions were negative for intracellular endoplasmic reticulum (Calnexin) and Golgi (GM130) markers indicating that the exosome-associated α-Synuclein detected was extracellular and not due to cell lysis (Supplementary Material, Fig. S4).

To further investigate this ATP13A2-enhanced externalization of exosome-associated α-Synuclein, we used density gradients to further purify exosomes from the media of α-Synuclein expressing HEK293 cells, with or without ATP13A2 overexpression. The floating of exosomes from the bottom of the density gradient eliminates contaminants from the subsequent analysis as large protein aggregates, which may co-sediment with exosomes sedimented by 100 000*g* centrifugation, do not subsequently float in a density gradient (41). Washed P100 fractions containing exosomes were loaded at the bottom of an OptiPrep density gradient and resolved by ultracentrifugation as has been described for enhanced exosomal purification (42). Fractions were collected and immunoblotted for a range of exosome markers [Alix, CD63, Flotillin, Hsp70 and Tsg101 (43)] as well as α-Synuclein (Fig. 8).

Elevated ATP13A2 expression resulted in a very large increase in exosomal α-Synuclein in a peak centred on fraction 4 (Fig. 8A). We examined whether elevated ATP13A2 expression changed the relative concentrations of exosomal markers within these α-Synuclein-containing fractions. Intriguingly, the fractionation pattern of the cytosolic molecular chaperone Hsp70 mirrored that of α-Synuclein with a large increase in a peak centred on fraction 4 that was completely dependent on ATP13A2 over-expression (Fig. 8C). Exosomal markers CD63 and Alix (43) also displayed large ATP13A2-dependent changes in fractions containing α-Synuclein (Fig. 8B and D). Flotillin and Tsg101 levels were also modulated by elevated ATP13A2 expression (Fig. 8E and F).

The role of ATP13A2 in the incorporation of α-Synuclein and exosomal markers into exosomes was further supported by assessing the impact of reduced ATP13A2 expression on this process. Exosomes from the media of HEK293 cells expressing α-Synuclein and either a vector control or an ATP13A2 shRNA knockdown plasmid were isolated (Supplementary Material, Fig. S5) and further purified by fractionation on a density gradient. ATP13A2 knockdown resulted in a >3-fold decrease in the level of exosomal α-Synuclein in the fraction 4-containing peak (Fig. 9A). This peak also displayed decreased levels of exosomal

Downloaded from http://hmg.oxfordjournals.org/ at University of New South Wales on October 13, 2014

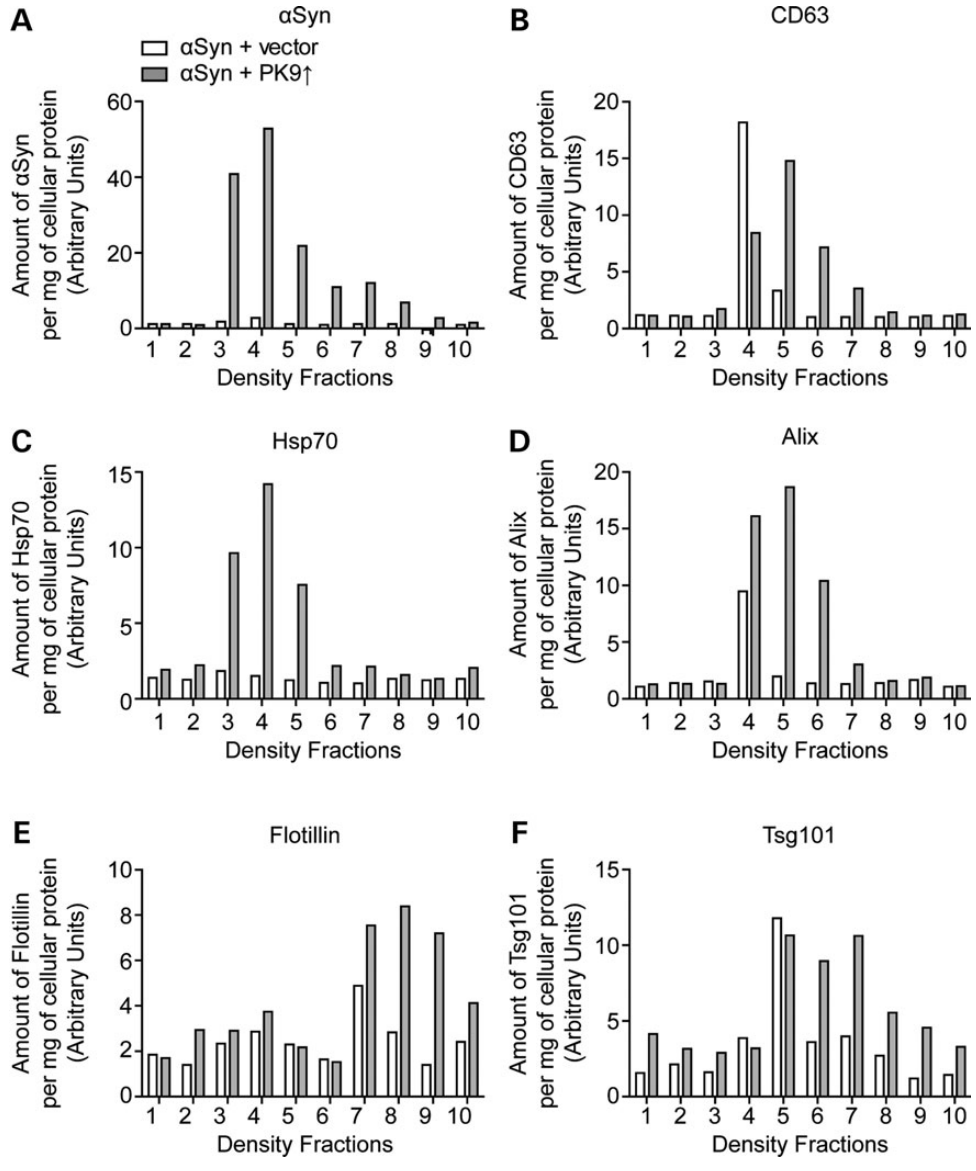

Figure 8. The effect of elevated ATP13A2 expression on exosomes containing human α-Synuclein (αSyn). Purified exosomes from HEK293 cells over-expressing αSyn, with vector control or ATP13A2 over-expression, were floated on a 0–50% OptiPrep density gradient (bottom loaded). Density gradient fractions (#1 lightest and # 10 heaviest) were then immunoprobed for (**A**) αSyn, (**B**) CD63, (**C**) Hsp70, (**D**) Alix, (**E**) Flotillin and (**F**) Tsg101. The immunoblot signal was quantified by densitometry analysis in ImageJ.

markers CD63 (>2-fold; Fig. 9B), Alix (3-fold; Fig. 9D), Flotillin (Fig. 9E) and Hsp70 (Fig. 9C).

DISCUSSION

Our data integrate previous observations that ATP13A2 expression is elevated in surviving DA neurons in sporadic PD patients (12) and that over-expression of ATP13A2 relieves α-Synuclein-induced cytotoxicity (9). We position ATP13A2 in MVBs, at the critical convergence point of the endosomal and autophagic pathways, acting to regulate Zn^{2+} homeostasis and influencing the exosome-associated externalization of α-Synuclein.

ATP13A2 plays a key role in zinc homeostasis

The P_5 subfamily of ATPases, of which ATP13A2 is a member, utilize ATP to transport inorganic cations such as metal ions (10,44). Loss of ATP13A2, whether through deletion of the yeast orthologue *YPK9*, or knockdown of human ATP13A2, conferred sensitivity to Zn^{2+} (Figs 1 and 2A). Furthermore, hONs derived from an ATP13A2$^{-/-}$ patient (11) lacked detectable ATP13A2 protein levels (Fig. 2C) and displayed significantly increased sensitivity to Zn^{2+} relative to control cells (Fig. 2D). Upon Zn^{2+} challenge, ATP13A2$^{-/-}$ patient hONs accumulated 60% more Zn^{2+} when compared with control hONs (Fig. 2F). Correspondingly, over-expression of either *YPK9* in yeast (Fig. 1) or human ATP13A2 in rat primary cortical neurons (Fig. 3) conferred resistance to zinc

Downloaded from http://hmg.oxfordjournals.org/ at University of New South Wales on October 13, 2014

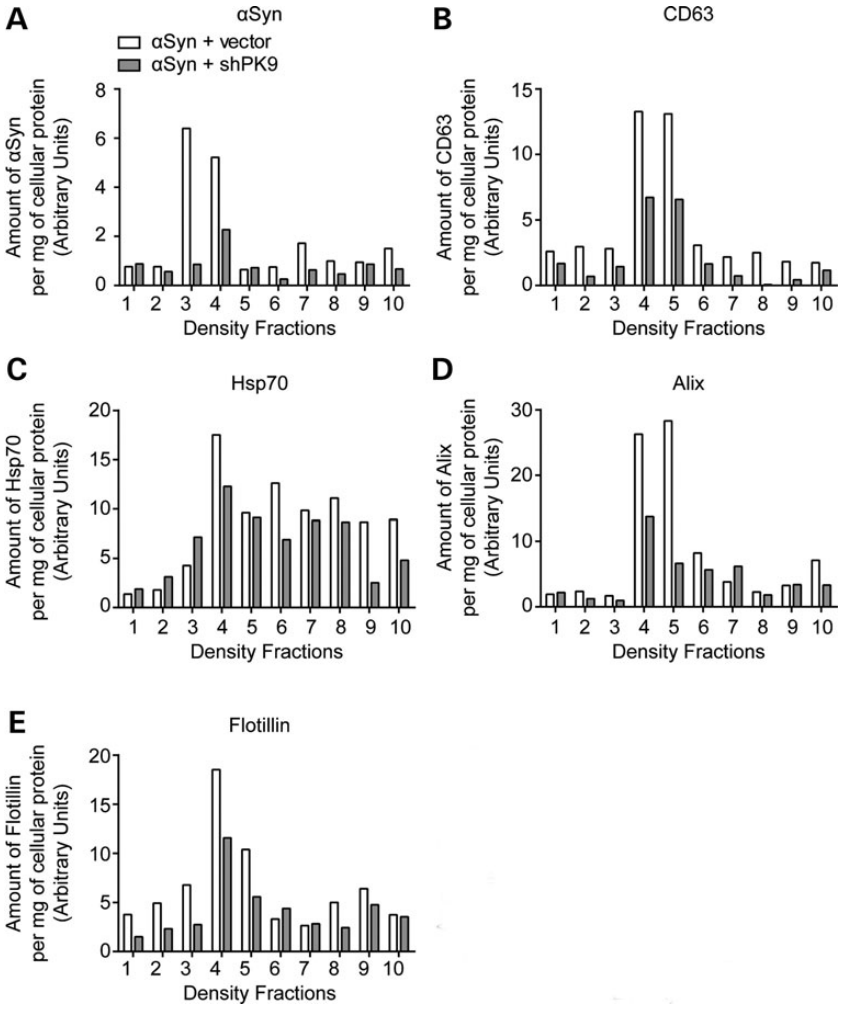

Figure 9. The effect of reduced ATP13A2 expression on exosomes containing human α-Synuclein (αSyn). Purified exosomes from HEK293 cells over-expressing αSyn, with vector control or ATP13A2 knockdown, were floated on a 0–50% OptiPrep density gradient (bottom loaded). Density gradient fractions (#1 lightest and # 10 heaviest) were then immunoprobed for (**A**) αSyn, (**B**) CD63, (**C**) Hsp70, (**D**) Alix and (**E**) Flotillin. The immunoblot signal was quantified by densitometry analysis in ImageJ.

challenges. Finally, ATP13A2 knockdown in two cell types robustly reduced vesicular zinc levels as detected by zinquin (Fig. 4C–E). Together these data strongly support the proposal that ATP13A2 plays a key role in zinc homeostasis, most likely, given it is a P_5 ATPase, by directly transporting Zn^{2+} from the cytosol into the MVB lumen. Further experimentation is required to directly demonstrate this function. By facilitating transport of cytosolic Zn^{2+} into the MVB lumen, ATP13A2 assists in maintaining cytosolic Zn^{2+} homeostasis but can additionally contribute to Zn^{2+} efflux from the cells as fusion of MVBs with the plasma membrane will release the ionic contents of the MVB lumen extracellularly. The loss of such a Zn^{2+} efflux would account for the significantly elevated levels of intracellular Zn^{2+} in ATP13A2$^{-/-}$ hONs when challenged with Zn^{2+} (Fig. 2F). An alternative explanation is that ATP13A2 expression negatively regulates uptake of extracellular Zn^{2+}, but this model would not account for the reduced zinquin staining upon decreased ATP13A2 expression.

Zinc plays an important role in neurobiology and is integral to the homeostasis of the central nervous system; a loss of zinc homeostasis can contribute to the degeneration of neurons that are sensitive to both deficiencies and excesses of zinc. Although total zinc levels are high in the brain, neurons maintain very low levels of cytosolic free zinc (estimated to be in the nanomolar range) through binding to metallothioneins and sequestration in vesicles (45,46). A range of zinc transporters and pumps contribute to zinc homeostasis by transporting Zn^{2+} across membranes of the plasma membrane and organelles/vesicular compartments (47). The loss in patients of ATP13A2′s capacity to facilitate Zn^{2+} transportation is likely to have two distinct detrimental consequences: perturbed MVB function owing to diminished MVB luminal zinc levels and correspondingly increased cytosolic zinc concentration. Elevated free zinc levels can potently inhibit mitochondrial membrane potential resulting in ROS generation (48) that triggers the release of metallothionein bound zinc to further elevate cytosolic zinc levels. Environmental zinc exposure has been associated with PD (49) and at least one PD model (MPTP/MPP^+) results in increased intracellular free zinc levels that contribute to the associated neurotoxicity (50).

ATP13A2 is less likely to play a significant role in Mn^{2+} homeostasis; neither ATP13A2 knockdown cells nor ATP

Downloaded from http://hmg.oxfordjournals.org/ at University of New South Wales on October 13, 2014

13A2$^{-/-}$ patient hONs displayed increased sensitivity to Mn^{2+} (Fig. 2B and E) and μ-XRF studies also found no difference in intracellular Mn^{2+} levels between ATP13A2$^{-/-}$ patient hONs and controls when treated with Mn^{2+} (Fig. 2G). It has been reported (51) that ATP13A2 over-expression can partially protect cultured cells from high Mn^{2+} levels (2 mM) raising the possibility that ATP13A2 may, at such high Mn^{2+} concentrations, be additionally capable of transporting Mn^{2+}. However, we found no significant difference in viability between ATP13A2$^{-/-}$ patient hONs and control hONs at Mn^{2+} levels as high as 5 mM (Fig. 2E).

ATP13A2 regulates zinc levels in MVBs

We found endogenous ATP13A2 in close association with the autophagosome marker LC3 (Fig. 5A and B), and this association was strongly enhanced in the presence of CQ, likely reflecting the dynamic nature of the interaction. ATP13A2-LC3-positive structures lacked lysosomal markers (Fig. 5D) and raised the possibility that ATP13A2 may reside on the autophagosomal membrane. However, ATP13A2 is not an obligate component of autophagosomes as we observed punctate LC3-positive structures that lacked ATP13A2. CQ treatment also revealed an association between ATP13A2 and the MVB markers LBPA and CD63 (Fig. 7). ATP13A2′s close association with both autophagosomes and MVBs is most consistent with ATP13A2 occupying the outer limiting membrane of MVBs that can fuse with autophagosomes to produce amphisomes (Fig. 10A) (32,52). The significant loss of zinquin-stained vesicular zinc in two different human cell lines with reduced ATP13A2 expression (Fig. 4C–E) indicates that ATP13A2 can function to regulate Zn^{2+} levels in the MVB lumen (Fig. 10B).

ATP13A2 has previously been assigned a lysosomal localization based on staining of over-expressed C-terminally tagged (V5–6xHis or GFP) ATP13A2 (12–15), and we also observed ATP13A2–V5–6xHis in the lysosome (Fig. 4A). However, we did not observe significant co-localization between endogenous ATP13A2 and the lysosome (Fig. 4B), raising the possibility that over-expressed tagged ATP13A2 is mislocalized, a prospect raised by the authors of the original ATP13A2-V5–6xHis/GFP constructs (12). Tagged proteins over-expressed in the secretory/endosomal system are susceptible to mislocalization by either sterically hindering C-terminal localization/retention sequences or saturating sorting machinery. In our studies, the elevated expression of untagged ATP13A2 did not result in lysosomal localization (Supplementary Material, Fig. S6), suggesting that the C-terminal tagging of ATP13A2 may be associated with its lysosomal localization.

MVBs can fuse with both autophagosomes and lysosomes and as such the autophagy–lysosomal pathway defects previously

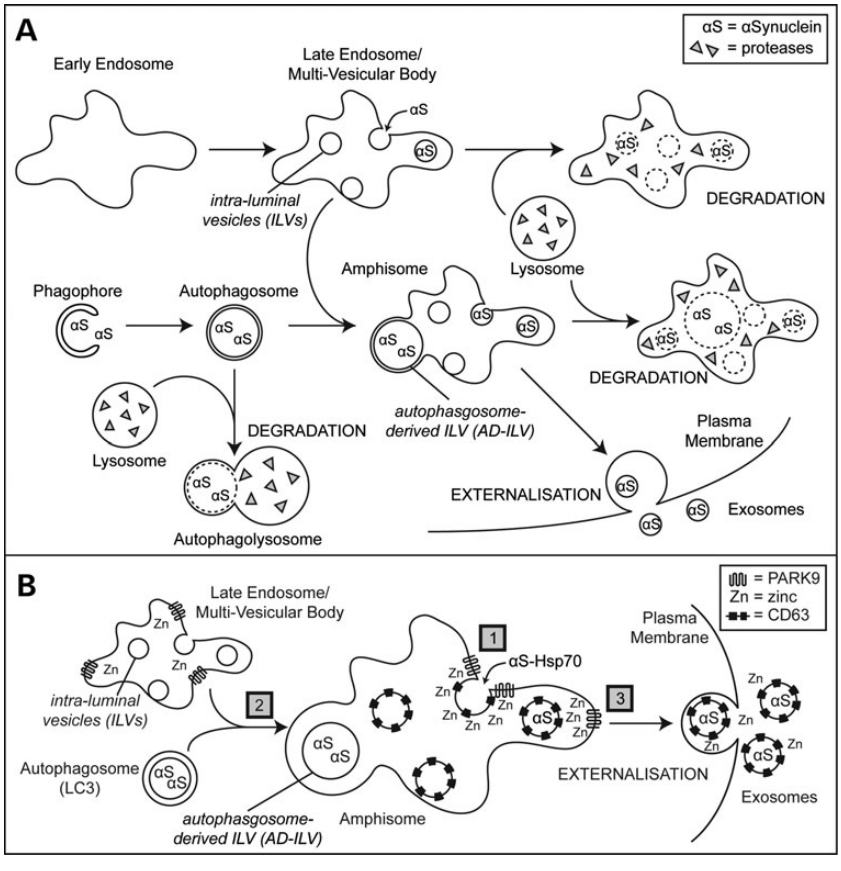

Figure 10. ATP13A2 functions in the endo-lysosomal pathway to reduce intracellular α-Synuclein levels by externalization in exosomes. Intracellular α-Synuclein levels can be reduced by lysosomal degradation via endosomal transport or autophagy, or by externalization in exosomes. (**B**) – (1) ATP13A2 may pump zinc to create a micro-environment to stabilize lipid clustering during ILV invagination, (2) ATP13A2 may increase vesicular zinc levels to aid in efficient autophagosome to MVB fusion or (3) ATP13A2 may pump zinc to create a micro-environment to sort ILVs to the plasma membrane resulting for release as exosomes.

Downloaded from http://hmg.oxfordjournals.org/ at University of New South Wales on October 13, 2014

associated with reduced ATP13A2 expression/function could arise as consequences of MVB dysfunction induced by ATP13A2 loss. Impaired fusion of MVBs with lysosomes would result in reduced delivery of lysosomal hydrolases, resulting in the observed decreased lysosomal proteolytic activity and reduced lysosomal clearance rates (14,15). Reduced fusion of MVBs with autophagosomes, or the subsequent fusion of amphisomes with lysosomes, could account for the impaired autophagosomal flux associated with reduced ATP13A2 function (15,53). Similarly, lysosomal delivery and degradation of dysfunctional mitochondria via mitophagy may also be impaired owing to decreased MVB function associated with reduced ATP13A2 activity (16). Additional lysosomal defects could result from Zn^{2+}-deficient MVBs fusing with lysosomes, potentially providing lysosomes with inadequate Zn^{2+} levels.

The role of ATP13A2 in α-Synuclein externalization

MVBs are dynamic organelles characterized by multiple ILVs enclosed within an outer limiting membrane. Initially regarded as purely prelysosomal structures along the degradative endosomal pathway, MVBs are now known to contribute to numerous endocytic and trafficking functions, including the externalization of ILVs as exosomes (33). MVBs can fuse with: (i) lysosomes to deliver ILVs for degradation, (ii) autophagosomes to produce autophagosome-derived ILVs (AD-ILVs) or (iii) the plasma membrane to release ILVs to the extracellular space as exosomes (Fig. 10A).

The fusion of MVBs with the plasma membrane will also release the ionic contents of the MVB lumen extracellularly, including any zinc that could in turn influence interneuronal signalling (54). Any resulting perturbations in intracellular zinc homeostasis could also interfere with normal neuronal signalling and contribute to PD.

The transport of Zn^{2+} into the MVB lumen is likely to convey functions beyond sequestering excess cytosolic Zn^{2+}. The metal plays an important role in the lumen of the late endosomal system as dyshomeostasis of Zn^{2+} transport to this compartment has been observed to affect membrane trafficking and/or sorting (55). By modulating luminal concentrations of Zn^{2+} within MVBs, ATP13A2 might play an important role in a range of functions that could include fusion of autophagosomes with MVBs, or regulating the biogenesis and/or sorting of ILVs within MVBs (Fig. 10B). Although a cytosolic protein, α-Synuclein may enter MVBs to produce α-Synuclein-containing ILVs via autophagy and/or late endosomal micro-autophagy (56). α-Synuclein could be engulfed by a phagophore forming an autophagosome that, upon fusion with an MVB, would result in an α-Synuclein-containing AD-ILV (Fig. 10A). In late endosomal micro-autophagy, cytosolic proteins can associate with molecular chaperones and the MVB limiting membrane and are incorporated into the nascent ILV lumen as it invaginates inward (56) (Fig. 10A). Identifying the proteins associated with α-Synuclein-containing exosomes, and determining whether their levels are modulated by ATP13A2 expression, provided valuable insights as to the mechanism involved.

Elevated expression of ATP13A2 resulted in a large increase in exosome-associated α-Synuclein (Fig. 8A) whose fractionation pattern was mirrored by that of Hsp70 (Fig. 8C), a molecular chaperone previously found in exosomes (57). Hsp70 has been shown to protect against α-Synuclein toxicity *in vitro*, to reduce the amount of α-Synuclein aggregates *in vivo* (58,59), and has been found to associate with externalized α-Synuclein (60). Given that Hsc70, the functional equivalent of Hsp70, was found to load ILVs with cytosolic proteins containing the peptide KFERQ, which includes α-Synuclein (56), it is possible that endosomal micro-autophagy is modulated by elevated ATP13A2 expression. ATP13A2 may produce zinc microenvironments in the MVB lumen that influence the clustering of lipid micro-domains and the sorting of α-Synuclein bound to Hsp70 into ILVs (Fig. 10B-1). Clustering of negatively charged lipid head groups within a micro-domain during invagination of a nascent ILV may be unfavourable owing to electrostatic repulsion and ATP13A2, providing luminal Zn^{2+} might help reduce this charge issue and allow more efficient lipid clustering, appropriate membrane curvature and ILV formation. An increased rate of ILV formation might permit enhanced endosomal micro-autophagy of α-Synuclein-Hsp70 and subsequent release as exosomes. Alternatively, modulation of MVB luminal zinc levels by ATP13A2 may enhance fusion of autophagosomes with MVBs (Fig. 10B-2) or impact the sorting of ILVs within MVBs between the alternative destinations of the plasma membrane and the lysosome (Fig. 10B-3). We observed that modulation of ATP13A2 expression caused corresponding changes of exosomal marker levels in purified exosomes (Figs 8 and 9) providing strong support that ATP13A2 plays a role in exosomal biogenesis.

Chemically induced lysosomal dysfunction, as reflected by large increases in both intracellular α-Synuclein and LC3-II levels, has been observed to result in an increase in α-Synuclein externalization (61). However, the process described by Alvarez-Erviti and co-workers (61) is distinct from that involving elevated ATP13A2 expression as, in contrast, we observed decreased intracellular α-Synuclein levels (Fig. 6B) and no increase in LC3-II levels (Supplementary Material, Fig. S3B), indicating no lysosomal dysfunction.

The role of ATP13A2 in Parkinson's disease

We have shown that elevated ATP13A2 expression results in decreased intracellular α-Synuclein levels and increased α-Synuclein externalization associated with exosomes. This is consistent with reduced ATP13A2 expression being associated with increased levels of intracellular α-Synuclein (15). Our data account for previous observations that elevated ATP13A2 expression suppressed α-Synuclein toxicity in several PD models including primary DA neurons (62) and that DA neurons still viable in the SNc of sporadic PD patients have been found to express ATP13A2 at 10-fold higher levels (12), whereas those cells either unable to compensate with elevated ATP13A2 expression or having naturally lower ATP13A2 expression levels may undergo degeneration (14,63). Our knockdown studies suggest that ATP13A2$^{-/-}$ patients would have an impaired capacity to produce exosomes and externalize α-Synuclein, which would likely contribute to their neurodegeneration.

Why would ATP13A2-dependent increased externalization of α-Synuclein via exosomes be beneficial to neurons when α-Synuclein delivered to MVBs via either autophagy or endosomal micro-autophagy could instead be delivered to the lysosome for degradation? This assumes that lysosomal delivery and

Downloaded from http://hmg.oxfordjournals.org/ at University of New South Wales on October 13, 2014

degradative capacity are fully functional in aging neurons. However, aging brains exhibit reduced lysosomal function (64) and human PD brain tissue shows an increased accumulation of autophagic vesicles (65,66), suggesting a possible significant impairment in their ability to fuse with lysosomes. α-Synuclein itself might be contributing to this lysosomal dysfunction as α-Synuclein has been demonstrated to impair the lysosomal enzyme glucocerebrosidase (GBA). GBA inhibition in turn caused an accumulation of α-Synuclein aggregates, which caused further lysosomal dysfunction and α-Synuclein accumulation (67). Externalization of α-Synuclein would bypass potentially insufficient neuronal degradative capacity or dysfunctional lysosomes to reduce intra-neuronal α-Synuclein levels and decrease α-Synuclein-associated toxicity. An impaired capacity to externalize α-Synuclein might therefore contribute to the neurodegeneration in ATP13A2$^{-/-}$ patients by increasing the degradative load on neuronal lysosomes, potentially enhancing lysosomal dysfunction and impairing the delivery and/or degradation of autophagosomes or dysfunctional mitochondria (16,53).

The detection of Lewy bodies in embryonic nigral neurons transplanted in PD patients suggested the possibility of host-to-graft disease propagation (68,69). α-Synuclein externalized in cell culture has been observed to negatively impact surrounding neurons (37), supporting the proposal that extracellular α-Synuclein plays an important role in disease progression by amplifying and spreading degenerative changes from neurons to surrounding tissues (70). ATP13A2-mediated externalization of α-Synuclein might benefit the exporting neuron by decreasing intracellular levels of toxic α-Synuclein but could this consequently transfer toxicity to neighbouring neurons and trigger their degeneration? This apparent enigma might be resolved by the possibility that both exosomal and non-exosomal mechanisms are contributing to the externalization of α-Synuclein and that extracellular α-Synuclein not within exosomes is at least partially responsible for the extracellular toxicity. Some of the toxic forms of extracellular α-Synuclein are clearly not contained within exosomes as their toxic effect was blunted with anti-α-Synuclein antibody (37), whereas bacterially produced recombinant α-Synuclein has imparted toxicity to both primary neurons and neurodegeneration in whole animal studies (71,72). Therefore, α-Synuclein externalized within exosomes may provide a benefit to the exporting neuron without conferring a detriment to neighbouring neurons.

Exosomes have been found to contain and transfer selected proteins, mRNA and microRNA into target cells and provide a powerful potential path of cell–cell communication as well as a promising therapeutic tool for multiple diseases. The rapidly expanding role of exosomes is being actively pursued within neurodegeneration, immunology, cancer biology and viral infection including HIV (73). Discovering how ATP13A2 and zinc influences MVBs and exosomes could well provide insights and potential therapeutic approaches not only for PD but also for a broad range of other diseases.

MATERIALS AND METHODS

Yeast culture conditions and spot assays for viability

Saccharomyces cerevisiae were cultured at 30°C in S media (0.5% w/v $(NH_4)_2SO_4$, 0.17% w/v yeast nitrogen base with amino acid selection) with glucose or galactose (2% w/v). *ypk9*Δ cells were transformed with *YPK9* galactose inducible over-expression plasmid (pBY011-*YPK9*) (9). Yeast media components were purchased from BD Sciences Difco (Australia).

Cell culture conditions

All cells were cultured at 37°C with 5% CO_2. HEK293 and SHSY5Y cells were cultured in DMEM/F12; SHSY5Y-αSyn cells were cultured in RPMI1640, with 10% FBS and 5 mM Glutamax. α-Synuclein over-expression was repressed with 5 μM doxycycline. SHSY5Y and SHSY5Y-αSyn cells were differentiated in 2% FBS in culture media with 10 μM retinoic acid. Cells were treated with 100 μM CQ for 1.5 h. Cortical neurons were cultured on poly-L-lysine-coated coverslips with Neurobasal media and B27 supplement. DMEM/F12, RPMI1640, Neurobasal media and other tissue culture components were purchased from Gibco Life Technologies (Australia). FBS GOLD was purchased from Quantum Scientific VWR (Australia). SHSY5Y cells were from American Type Culture Collection (USA), HEK293FT cells were a kind gift from Professor David James (Garvan Institute of Medical Research, Australia) and SHSY5Y-αSyn cells were a kind gift from Dr Kostas Vekrellis (University of Athens, Greece).

Establishment and culture of hONs has been described (11). Briefly, primary olfactory cells were cultured from a nose biopsy of the proband and an age- and sex-matched control subject with enzymatic dissociation and BM cyclin treatment. Neurospheres were generated by growing primary olfactory cells on a poly-L-lysine-coated plate with supplement of 25 nM basic fibroblast growth factor, 50 nM epidermal growth factor and ITS and then cultured in DMEM containing 10% FBS and antibiotics.

ATP13A2 antibody production

Rabbit polyclonal antibodies were raised against human ATP13A2 (amino acids 72–256 that lacked identity with other human protein/P-type ATPases) and affinity-purified against recombinant ATP13A2 protein. Polyclonal antibody production was conducted by IMVS Veterinary Services (SA, Australia).

Production of ATP13A2 knockdown/over-expression cell lines

siRNA targeting PARK9 was purchased from Dhamacon (Australia). For the knockdown of ATP13A2, shRNA against ATP13A2 was cloned into the lentiviral vector pLL5.0 (74) to produce the plasmid pAC1085. For the over-expression of ATP13A2, full-length ATP13A2 [pENTR-ATP13A2 (9)] was sub-cloned into pLenti6/V5-Dest with gateway technology (Life Technologies, Australia). The empty pLL5.0 vector backbone was used create vector control cells. For lentivirus production, constructs and lentiviral packaging plasmids (pMD2G, pMDLg/pRE and pRSV.Rev) (75) were transfected into HEK293 cells using Lipofectamine 2000 (Life Technologies).

For the knockdown of PARK9, SHSY5Y cells were transfected with PARK9 siRNA by Amaxa electroporation nucleofection (Lonza, Australia). siRNA-mediated PARK9 knockdown was assessed by immunoblotting. For the creation of stable cell

Downloaded from http://hmg.oxfordjournals.org/ at University of New South Wales on October 13, 2014

lines, lentivirus was collected and concentrated using Amicon column centrifugation. SHSY5Y and SHSY5Y-aSyn cells were infected with lentivirus for 24 h. Stably infected cells were selected for using 2 μg/ml blasticidin. Fluorescence-activated cell sorting (FACS) confirmation and western blots were conducted to assess PARK9 knockdown/over-expression.

Synchrotron elemental analysis of hONs

Sterilized silicon nitride windows (1.5 × 1.5 mM^2 × 500 nm) (Silson, UK) were seeded with 3 × 10^4 hONS cells in 6-well plates and incubated for 24 h, as previously described (76,77). Cells were then treated with 0.1 mM $ZnCl_2$ or 1 mM $MnCl_2$ for 24 h before fixation. X-ray fluorescence elemental distribution maps of single cells were recorded on the XFM beam-line at the Australian Synchrotron (Victoria, Australia).

A monochromatic 9.9-keV X-ray beam was focused using a 'high resolution' zone plate, and the fluorescence signal was collected using a single-element silicon drift energy dispersive detector (Vortex EX, SII Nanotechnology, Northridge, CA, USA) for 1 s per spatial point. Individual cells were located using images obtained from an optical microscope positioned in the beam-line downstream from the sample.

The fluorescence spectrum at each spatial point was fit to Gaussians, modified by the addition of a step function and a tailing function to describe mostly incomplete charge collection and other detector artefacts. The analysis was performed using MAPS software (78) standardized by fitting to known spectra from NIST (National Bureau of Standards, Gaithersburg, MD, USA). Elemental area content (counts/cm^2) are presented as the mean and the standard deviation in the mean.

Viability assays

SHSY5Y cells were seeded at 2 × 10^4 cells/well in 96-well plates, differentiated for 48 h then treated with various stress conditions for a further 48 h. Cell viability was assessed by alamarBlue (Life Technologies, Australia). hONs viability assays were performed in 24-well plates seeded at 5 × 10^4 cells/well in media for 24 h. hONs were grown in serum-free media for an additional 24 h, treated with $ZnCl_2$ for 48 h, and cell viability was assessed by MTT assay.

SDS–PAGE gel and immunoblotting

Proteins were extracted with HES buffer and concentration determined by a BCA assay (Pierce, IL, USA). Protein samples were separated by SDS–PAGE and transferred onto nitrocellulose or PVDF membrane. Immunoblots were incubated with primary and secondary antibody before development with HRP chemiluminescence (Millipore, Australia). Proteins were extracted with HES buffer (2% w/v SDS, 20 mM HEPES, 1 mM EDTA, 250 mM sucrose, Roche cOmplete™ protease inhibitors, pH 7.4). Blots were blocked with 10% milk in TTBS (Tris-buffered Saline, 0.1% Tween) and incubated with primary antibodies for 24 h at 4°C followed by secondary antibodies for 1 h at room temperature. Blots were washed at least three times in TTBS after incubations.

Antibodies against α-Synuclein, β-Tubulin, CD63, LC3 and LAMP1 were purchased from BD Laboratories, Iowa Monoclonal Bank, BioLegend, MBL and Iowa Monoclonal Bank, respectively. Antibodies against LBPA were a kind gift from Dr Robert Parton (University of Queensland, Australia).

Indirect immunofluorescence microscopy

Cells cultured on coverslips were fixed in 4% PFA, blocked and incubated with primary and secondary antibody. Coverslips were washed after incubations and mounted onto slides for microscopy. For zinquin analysis, fixed coverslips were incubated with 20 μM zinquin for 30 min, washed and mounted for microscopy. Fluorescent images were taken on a Zeiss Upright microscope using Axiovision Version 4.8, or a N-SIM Super Resolution Microscope (Nikon) for Figs. 4B and 7B.

Zinquin fluorescence-activated cell sorting

HEK293 cells were seeded in triplicate at 20 × 10^4 cells per well in a six-well plate. Cells were incubated for 16 h at 37°C prior to transfection with appropriate plasmids. Cells were then incubated for a further 48 h at 37°C. Culture media was then replaced with fresh media containing zinquin at a final concentration of 20 μM and cells incubated for 1 h at 37°C. Cells were then harvested and resuspended in 500 μl FACS buffer (2 mM EDTA, 25 mM HEPES, 1% FBS in PBS), and 10,000 cells per sample were analysed in a 7 Laser SORP LSRII FACS machine (BD Biosciences). Zinquin was detected with a 355-nm laser, and GFP (the ATP13A2 shRNA knockdown plasmid shPK9 was marked with GFP) was detected with a 514-nm laser. Data were then analysed using BD coherent and BDFACSDiva software version 6.1.3 (BD Biosciences) and plotted as medium fluorescent intensity. For cells transfected with shPK9, zinquin fluorescence was only measured in cells that also displayed a GFP signal (an indication of shPK9 expression).

Exosome purification and density analysis

HEK293 cells were seeded into 15 cm dishes and then transfected with appropriate plasmids using Lipofectamine 2000 (Life Technologies). Media was changed 16 h after transfection to exosome-free medium (complete medium containing exosome-depleted FCS), and cells were grown for a further 48 h. Cell-free culture media was harvested as previously described (79). Culture supernatants were collected, and cellular debris was removed by centrifugation at 300 g for 10 min. The supernatant was centrifuged at 5000 g for 30 min at 4°C. The supernatant was collected and centrifuged at 100,000 g for 2 h to pellet exosomes. Exosome pellets were resuspended and washed in PBS before being re-centrifuged at 100,000 g to pellet exosomes. The final exosome-containing pellet was resuspended in PBS and used for either immunoanalysis or density gradient fractionation.

For gradient fractionation of 100,000 g exosomal pellets, a discontinuous step-gradient of 0–50% OptiPrep (AxisShield) was used. The 100,000 g exosomal pellets were resuspended in 50% OptiPrep and step-gradients of OptiPrep in 10% decreases were layered on top. The step gradients were centrifuged at 100,000 g for 18 h at 4°C in a SW41 rotor, and fractions of 400 μl were harvested. Each density gradient fraction was diluted with PBS before being re-pelleted at 100,000 g for 1 h,

Downloaded from http://hmg.oxfordjournals.org/ at University of New South Wales on October 13, 2014

and the resulting exosomes pellets were resuspended in PBS for further analysis by immunoblot. An Auto-Densi Flow machine (Labconco, USA) was used to create and harvest all density gradients.

Imaging and statistical analysis

Densitometry and microscopy fluorescence intensity were conducted using Macbiophotonics ImageJ (http://www.macbiophotonics.ca/imagej). Neurite length was measured using Simple Neurite Tracer in Fiji (http://pacific.mpi-cbg.de/wiki/index.php/Fiji). Microscopy images were pseudo-coloured and overlayed using Photoshop (Adobe). Graphing and statistical analysis were conducted in Prism (GraphPad).

SUPPLEMENTARY MATERIAL

Supplementary Material is available at *HMG* online.

ACKNOWLEDGEMENTS

We thank Peter Zalewski for zinquin, Eva Kovacs for pLL5.0 and shRNA advice, Tristan Tan for help with the Nikon N-SIM Super Resolution Microscope and Kostas Vekrellis for the SHSY5Y-αSyn cells and Ornella Tolhurst for help creating SHSY5Y-V5-tagged ATP13A2 cells. We thank Adam Cole and Hovik Farghaian for providing us rat primary neurons. We also thank the beam-line scientists Martin de Jonge, David Paterson and Daryl Howard at the Australian Synchrotron for their help.

Conflict of Interest statement. None declared.

FUNDING

This work was supported by a project grant from the NHMRC. S.M.Y.K. was supported by the National Health and Medical Research Council and the Estate of the Late Olga Mabel Woolger. B.K.K.C. was supported by an Australian Post-graduate Award. J.B.A. was supported by the Australian Research Council and P.A.L. was supported by the Australian Research Council, including a Professorial Fellowship. C.M.S. is supported by a National Health and Medical Research Council Clinical Practitioner Fellowship and the Ramsay Health Teaching Research Fund. Work at the Australian Synchrotron was supported by the Australian Synchrotron Access Program.

REFERENCES

1. Braak, H., Del Tredici, K., Rub, U., de Vos, R.A., Jansen Steur, E.N. and Braak, E. (2003) Staging of brain pathology related to sporadic Parkinson's disease. *Neurobiol. Aging*, **24**, 197–211.
2. Spillantini, M.G., Schmidt, M.L., Lee, V.M., Trojanowski, J.Q., Jakes, R. and Goedert, M. (1997) Alpha-synuclein in Lewy bodies. *Nature*, **388**, 839–840.
3. Tan, E.K. and Skipper, L.M. (2007) Pathogenic mutations in Parkinson disease. *Hum. Mutat.*, **28**, 641–653.
4. Polymeropoulos, M.H., Lavedan, C., Leroy, E., Ide, S.E., Dehejia, A., Dutra, A., Pike, B., Root, H., Rubenstein, J., Boyer, R. *et al.* (1997) Mutation in the alpha-synuclein gene identified in families with Parkinson's disease. *Science*, **276**, 2045–2047.
5. Satake, W., Nakabayashi, Y., Mizuta, I., Hirota, Y., Ito, C., Kubo, M., Kawaguchi, T., Tsunoda, T., Watanabe, M., Takeda, A. *et al.* (2009) Genome-wide association study identifies common variants at four loci as genetic risk factors for Parkinson's disease. *Nat. Genet.*, **41**, 1303–1307.
6. Simon-Sanchez, J., Schulte, C., Bras, J.M., Sharma, M., Gibbs, J.R., Berg, D., Paisan-Ruiz, C., Lichtner, P., Scholz, S.W., Hernandez, D.G. *et al.* (2009) Genome-wide association study reveals genetic risk underlying Parkinson's disease. *Nat. Genet.*, **41**, 1308–1312.
7. Wu, F., Poon, W.S., Lu, G., Wang, A., Meng, H., Feng, L., Li, Z. and Liu, S. (2009) Alpha-synuclein knockdown attenuates MPP+ induced mitochondrial dysfunction of SH-SY5Y cells. *Brain Res.*, **1292**, 173–179.
8. Xilouri, M., Vogiatzi, T., Vekrellis, K. and Stefanis, L. (2008) alpha-synuclein degradation by autophagic pathways: a potential key to Parkinson's disease pathogenesis. *Autophagy*, **4**, 917–919.
9. Gitler, A.D., Chesi, A., Geddie, M.L., Strathearn, K.E., Hamamichi, S., Hill, K.J., Caldwell, K.A., Caldwell, G.A., Cooper, A.A., Rochet, J.C. *et al.* (2009) Alpha-synuclein is part of a diverse and highly conserved interaction network that includes PARK9 and manganese toxicity. *Nat. Genet.*, **41**, 308–315.
10. Schultheis, P.J., Hagen, T.T., O'Toole, K.K., Tachibana, A., Burke, C.R., McGill, D.L., Okunade, G.W. and Shull, G.E. (2004) Characterization of the P5 subfamily of P-type transport ATPases in mice. *Biochem. Biophys. Res. Commun.*, **323**, 731–738.
11. Park, J.S., Mehta, P., Cooper, A.A., Veivers, D., Heimbach, A., Stiller, B., Kubisch, C., Fung, V.S., Krainc, D., Mackay-Sim, A. *et al.* (2011) Pathogenic effects of novel mutations in the P-type ATPase ATP13A2 (PARK9) causing Kufor-Rakeb syndrome, a form of early-onset parkinsonism. *Hum Mutat*, **32**, 956–964.
12. Ramirez, A., Heimbach, A., Grundemann, J., Stiller, B., Hampshire, D., Cid, L.P., Goebel, I., Mubaidin, A.F., Wriekat, A.L., Roeper, J. *et al.* (2006) Hereditary parkinsonism with dementia is caused by mutations in ATP13A2, encoding a lysosomal type 5 P-type ATPase. *Nat. Genet.*, **38**, 1184–1191.
13. Ramonet, D., Podhajska, A., Stafa, K., Sonnay, S., Trancikova, A., Tsika, E., Pletnikova, O., Troncoso, J.C., Glauser, L. and Moore, D.J. (2011) PARK9-associated ATP13A2 localizes to intracellular acidic vesicles and regulates cation homeostasis and neuronal integrity. *Hum. Mol. Genet.*, **21**, 1725–1743.
14. Dehay, B., Ramirez, A., Martinez-Vicente, M., Perier, C., Canron, M.-H., Doudnikoff, E., Vital, A., Vila, M., Klein, C. and Bezard, E. (2012) Loss of P-type ATPase ATP13A2/PARK9 function induces general lysosomal deficiency and leads to Parkinson disease neurodegeneration. *Proc. Natl. Acad. Sci. USA*, **109**, 9611–9616.
15. Usenovic, M., Tresse, E., Mazzulli, J.R., Taylor, J.P. and Krainc, D. (2012) Deficiency of ATP13A2 leads to lysosomal dysfunction, alpha-synuclein accumulation, and neurotoxicity. *J. Neurosci.*, **32**, 4240–4246.
16. Grunewald, A., Arns, B., Seibler, P., Rakovic, A., Munchau, A., Ramirez, A., Sue, C.M. and Klein, C. (2012) ATP13A2 mutations impair mitochondrial function in fibroblasts from patients with Kufor-Rakeb syndrome. *Neurobiol. Aging.*, **33**, 1843, e1–e7.
17. Klionsky, D.J., Baehrecke, E.H., Brumell, J.H., Chu, C.T., Codogno, P., Cuervo, A.M., Debnath, J., Deretic, V., Elazar, Z., Eskelinen, E.L. *et al.* (2011) A comprehensive glossary of autophagy-related molecules and processes (2nd edition). *Autophagy*, **7**, 1273–1294.
18. Williams, A., Jahreiss, L., Sarkar, S., Saiki, S., Menzies, F.M., Ravikumar, B. and Rubinsztein, D.C. (2006) Aggregate-prone proteins are cleared from the cytosol by autophagy: therapeutic implications. *Curr. Top. Dev. Biol.*, **76**, 89–101.
19. Hara, T., Nakamura, K., Matsui, M., Yamamoto, A., Nakahara, Y., Suzuki-Migishima, R., Yokoyama, M., Mishima, K., Saito, I., Okano, H. *et al.* (2006) Suppression of basal autophagy in neural cells causes neurodegenerative disease in mice. *Nature*, **441**, 885–889.
20. Klionsky, D.J. and Emr, S.D. (2000) Autophagy as a regulated pathway of cellular degradation. *Science*, **290**, 1717–1721.
21. Vogiatzi, T., Xilouri, M., Vekrellis, K. and Stefanis, L. (2008) Wild type alpha-synuclein is degraded by chaperone-mediated autophagy and macroautophagy in neuronal cells. *J. Biol. Chem.*, **283**, 23542–23556.
22. Schneider, A. and Simons, M. (2013) Exosomes: vesicular carriers for intercellular communication in neurodegenerative disorders. *Cell Tissue Res.*, **352**, 33–47.
23. Aitken, J.B., Carter, E.A., Eastgate, H., Hackett, M.J., Harris, H.H., Levina, A., Lee, Y.-C., Chen, C.-I., Lai, B., Vogt, S. *et al.* (2010) Biomedical applications of X-ray absorption and vibrational spectroscopic microscopies

Downloaded from http://hmg.oxfordjournals.org/ at University of New South Wales on October 13, 2014

in obtaining structural information from complex systems. *Radiat. Phys. Chem.*, **79**, 176–184.
24. King, M., Nafar, F., Clarke, J. and Mearow, K. (2009) The small heat shock protein Hsp27 protects cortical neurons against the toxic effects of beta-amyloid peptide. *J. Neurosci. Res.*, **87**, 3161–3175.
25. Yang, Y., Kawataki, T., Fukui, K. and Koike, T. (2007) Cellular Zn2+ chelators cause "dying-back" neurite degeneration associated with energy impairment. *J. Neurosci. Res.*, **85**, 2844–2855.
26. Snitsarev, V., Budde, T., Stricker, T.P., Cox, J.M., Krupa, D.J., Geng, L. and Kay, A.R. (2001) Fluorescent detection of Zn(2+)-rich vesicles with Zinquin: mechanism of action in lipid environments. *Biophys. J.*, **80**, 1538–1546.
27. Zalewski, P.D., Forbes, I.J. and Betts, W.H. (1993) Correlation of apoptosis with change in intracellular labile Zn(II) using zinquin [(2-methyl-8-p-toluenesulphonamido-6-quinolyloxy)acetic acid], a new specific fluorescent probe for Zn(II). *Biochem. J.*, **296** (Pt 2), 403–408.
28. Lee, S.J., Cho, K.S. and Koh, J.Y. (2009) Oxidative injury triggers autophagy in astrocytes: the role of endogenous zinc. *Glia*, **57**, 1351–1361.
29. Vekrellis, K., Xilouri, M., Emmanouilidou, E. and Stefanis, L. (2009) Inducible over-expression of wild type alpha-synuclein in human neuronal cells leads to caspase-dependent non-apoptotic death. *J. Neurochem.*, **109**, 1348–1362.
30. Seglen, P.O., Grinde, B. and Solheim, A.E. (1979) Inhibition of the lysosomal pathway of protein degradation in isolated rat hepatocytes by ammonia, methylamine, chloroquine and leupeptin. *Eur. J. Biochem.*, **95**, 215–225.
31. Kabeya, Y., Mizushima, N., Ueno, T., Yamamoto, A., Kirisako, T., Noda, T., Kominami, E., Ohsumi, Y. and Yoshimori, T. (2000) LC3, a mammalian homologue of yeast Apg8p, is localized in autophagosome membranes after processing. *EMBO J.*, **19**, 5720–5728.
32. Fader, C.M. and Colombo, M.I. (2009) Autophagy and multivesicular bodies: two closely related partners. *Cell Death Differ.*, **16**, 70–78.
33. Simons, M. and Raposo, G. (2009) Exosomes—vesicular carriers for intercellular communication. *Curr. Opin. Cell Biol.*, **21**, 575–581.
34. Babst, M. (2011) MVB vesicle formation: ESCRT-dependent, ESCRT-independent and everything in between. *Curr. Opin. Cell Biol.*, **23**, 452–457.
35. Mobius, W., van Donselaar, E., Ohno-Iwashita, Y., Shimada, Y., Heijnen, H.F., Slot, J.W. and Geuze, H.J. (2003) Recycling compartments and the internal vesicles of multivesicular bodies harbor most of the cholesterol found in the endocytic pathway. *Traffic*, **4**, 222–231.
36. Escola, J.M., Kleijmeer, M.J., Stoorvogel, W., Griffith, J.M., Yoshie, O. and Geuze, H.J. (1998) Selective enrichment of tetraspan proteins on the internal vesicles of multivesicular endosomes and on exosomes secreted by human B-lymphocytes. *J. Biol. Chem.*, **273**, 20121–20127.
37. Emmanouilidou, E., Melachroinou, K., Roumeliotis, T., Garbis, S.D., Ntzouni, M., Margaritis, L.H., Stefanis, L. and Vekrellis, K. (2010) Cell-produced alpha-synuclein is secreted in a calcium-dependent manner by exosomes and impacts neuronal survival. *J. Neurosci.*, **30**, 6838–6851.
38. Gross, J.C., Chaudhary, V., Bartscherer, K. and Boutros, M. (2012) Active Wnt proteins are secreted on exosomes. *Nat. Cell Biol.*, **14**, 1036–1045.
39. Ohno, S., Takanashi, M., Sudo, K., Ueda, S., Ishikawa, A., Matsuyama, N., Fujita, K., Mizutani, T., Ohgi, T., Ochiya, T. *et al.* (2013) Systemically injected exosomes targeted to EGFR deliver antitumor microRNA to breast cancer cells. *Mol. Ther.*, **21**, 185–191.
40. Fruhbeis, C., Frohlich, D. and Kramer-Albers, E.M. (2012) Emerging roles of exosomes in neuron-glia communication. *Front. Physiol.*, **3**, 119.
41. Thery, C., Zitvogel, L. and Amigorena, S. (2002) Exosomes: composition, biogenesis and function. *Nat. Rev. Immunol.*, **2**, 569–579.
42. Coleman, B.M., Hanssen, E., Lawson, V.A. and Hill, A.F. (2012) Prion-infected cells regulate the release of exosomes with distinct ultrastructural features. *FASEB J.*, **26**, 4160–4173.
43. Mathivanan, S., Fahner, C.J., Reid, G.E. and Simpson, R.J. (2012) ExoCarta 2012: database of exosomal proteins, RNA and lipids. *Nucleic Acids Res.*, **40**, D1241–D1244.
44. Palmgren, M.G. and Nissen, P. (2011) P-type ATPases. *Annu. Rev. Biophys.*, **40**, 243–266.
45. Maret, W. (2008) Metallothionein redox biology in the cytoprotective and cytotoxic functions of zinc. *Exp. Gerontol.*, **43**, 363–369.
46. Maret, W. (2006) Zinc coordination environments in proteins as redox sensors and signal transducers. *Antioxid. Redox Signal*, **8**, 1419–1441.
47. Sensi, S.L., Paoletti, P., Bush, A.I. and Sekler, I. (2009) Zinc in the physiology and pathology of the CNS. *Nat. Rev. Neurosci.*, **10**, 780–791.
48. Dineley, K.E., Richards, L.L., Votyakova, T.V. and Reynolds, I.J. (2005) Zinc causes loss of membrane potential and elevates reactive oxygen species in rat brain mitochondria. *Mitochondrion*, **5**, 55–65.
49. Pals, P., Van Everbroeck, B., Grubben, B., Viaene, M.K., Dom, R., van der Linden, C., Santens, P., Martin, J.J. and Cras, P. (2003) Case-control study of environmental risk factors for Parkinson's disease in Belgium. *Eur. J. Epidemiol.*, **18**, 1133–1142.
50. Sheline, C.T., Zhu, J., Zhang, W., Shi, C. and Cai, A.L. (2013) Mitochondrial inhibitor models of Huntington's disease and Parkinson's disease induce zinc accumulation and are attenuated by inhibition of zinc neurotoxicity in vitro or in vivo. *Neurodegener. Dis.*, **11**, 49–58.
51. Tan, J., Zhang, T., Jiang, L., Chi, J., Hu, D., Pan, Q., Wang, D. and Zhang, Z. (2011) Regulation of intracellular manganese homeostasis by Kufor-Rakeb syndrome-associated ATP13A2 protein. *J. Biol. Chem.*, **286**, 29654–29662.
52. Filimonenko, M., Stuffers, S., Raiborg, C., Yamamoto, A., Malerod, L., Fisher, E.M., Isaacs, A., Brech, A., Stenmark, H. and Simonsen, A. (2007) Functional multivesicular bodies are required for autophagic clearance of protein aggregates associated with neurodegenerative disease. *J. Cell Biol.*, **179**, 485–500.
53. Gusdon, A.M., Zhu, J., Van Houten, B. and Chu, C.T. (2012) ATP13A2 regulates mitochondrial bioenergetics through macroautophagy. *Neurobiol. Dis.*, **45**, 962–972.
54. Nakashima, A.S. and Dyck, R.H. (2009) Zinc and cortical plasticity. *Brain Res. Rev.*, **59**, 347–373.
55. Kobayashi, T., Beuchat, M.H., Lindsay, M., Frias, S., Palmiter, R.D., Sakuraba, H., Parton, R.G. and Gruenberg, J. (1999) Late endosomal membranes rich in lysobisphosphatidic acid regulate cholesterol transport. *Nat. Cell Biol.*, **1**, 113–118.
56. Sahu, R., Kaushik, S., Clement, C.C., Cannizzo, E.S., Scharf, B., Follenzi, A., Potolicchio, I., Nieves, E., Cuervo, A.M. and Santambrogio, L. (2011) Microautophagy of cytosolic proteins by late endosomes. *Dev. Cell*, **20**, 131–139.
57. Zhan, R., Leng, X., Liu, X., Wang, X., Gong, J., Yan, L., Wang, L., Wang, Y., Wang, X. and Qian, L.-J. (2009) Heat shock protein 70 is secreted from endothelial cells by a non-classical pathway involving exosomes. *Biochem. Biophys. Res. Commun.*, **387**, 229–233.
58. Dedmon, M.M., Christodoulou, J., Wilson, M.R. and Dobson, C.M. (2005) Heat shock protein 70 inhibits alpha-synuclein fibril formation via preferential binding to prefibrillar species. *J. Biol. Chem.*, **280**, 14733–14740.
59. Klucken, J., Shin, Y., Masliah, E., Hyman, B.T. and McLean, P.J. (2004) Hsp70 reduces alpha-Synuclein aggregation and toxicity. *J. Biol. Chem.*, **279**, 25497–25502.
60. Danzer, K.M., Ruf, W.P., Putcha, P., Joyner, D., Hashimoto, T., Glabe, C., Hyman, B.T. and McLean, P.J. (2011) Heat-shock protein 70 modulates toxic extracellular α-synuclein oligomers and rescues trans-synaptic toxicity. *FASEB J.*, **25**, 326–336.
61. Alvarez-Erviti, L., Seow, Y., Schapira, A.H., Gardiner, C., Sargent, I.L., Wood, M.J. and Cooper, J.M. (2011) Lysosomal dysfunction increases exosome-mediated alpha-synuclein release and transmission. *Neurobiol. Dis.*, **42**, 360–367.
62. Gitler, A.D., Bevis, B.J., Shorter, J., Strathearn, K.E., Hamamichi, S., Su, L.J., Caldwell, K.A., Caldwell, G.A., Rochet, J.C., McCaffery, J.M. *et al.* (2008) The Parkinson's disease protein alpha-synuclein disrupts cellular Rab homeostasis. *Proc. Natl. Acad. Sci. USA*, **105**, 145–150.
63. Murphy, K.E., Cottle, L., Gysbers, A.M., Cooper, A.A. and Halliday, G.M. (2013) ATP13A2 (PARK9) protein levels are reduced in brain tissue of cases with Lewy bodies. *Acta Neuropathol. Commun.*, **1**, 11.
64. Cuervo, A.M. and Dice, J.F. (2000) When lysosomes get old. *Exp. Gerontol.*, **35**, 119–131.
65. Anglade, P., Vyas, S., Javoy-Agid, F., Herrero, M.T., Michel, P.P., Marquez, J., Mouatt-Prigent, A., Ruberg, M., Hirsch, E.C. and Agid, Y. (1997) Apoptosis and autophagy in nigral neurons of patients with Parkinson's disease. *Histol. Histopathol.*, **12**, 25–31.
66. Zhu, J.H., Guo, F., Shelburne, J., Watkins, S. and Chu, C.T. (2003) Localization of phosphorylated ERK/MAP kinases to mitochondria and autophagosomes in Lewy body diseases. *Brain Pathol.*, **13**, 473–481.
67. Mazzulli, J.R., Xu, Y.H., Sun, Y., Knight, A.L., McLean, P.J., Caldwell, G.A., Sidransky, E., Grabowski, G.A. and Krainc, D. (2011) Gaucher disease glucocerebrosidase and alpha-synuclein form a bidirectional pathogenic loop in synucleinopathies. *Cell*, **146**, 37–52.

Downloaded from http://hmg.oxfordjournals.org/ at University of New South Wales on October 13, 2014

68. Kordower, J.H., Chu, Y., Hauser, R.A., Freeman, T.B. and Olanow, C.W. (2008) Lewy body-like pathology in long-term embryonic nigral transplants in Parkinson's disease. *Nat. Med.*, **14**, 504–506.
69. Li, J.Y., Englund, E., Holton, J.L., Soulet, D., Hagell, P., Lees, A.J., Lashley, T., Quinn, N.P., Rehncrona, S., Bjorklund, A. *et al.* (2008) Lewy bodies in grafted neurons in subjects with Parkinson's disease suggest host-to-graft disease propagation. *Nat. Med.*, **14**, 501–503.
70. Brundin, P., Melki, R. and Kopito, R. (2010) Prion-like transmission of protein aggregates in neurodegenerative diseases. *Nat. Rev. Mol. Cell Biol.*, **11**, 301–307.
71. Luk, K.C., Kehm, V., Carroll, J., Zhang, B., O'Brien, P., Trojanowski, J.Q. and Lee, V.M. (2012) Pathological alpha-synuclein transmission initiates Parkinson-like neurodegeneration in nontransgenic mice. *Science*, **338**, 949–953.
72. Volpicelli-Daley, L.A., Luk, K.C., Patel, T.P., Tanik, S.A., Riddle, D.M., Stieber, A., Meaney, D.F., Trojanowski, J.Q. and Lee, V.M. (2011) Exogenous alpha-synuclein fibrils induce Lewy body pathology leading to synaptic dysfunction and neuron death. *Neuron*, **72**, 57–71.
73. Pegtel, D.M., van de Garde, M.D. and Middeldorp, J.M. (2011) Viral miRNAs exploiting the endosomal-exosomal pathway for intercellular cross-talk and immune evasion. *Biochem. Biophys. Acta*, **1809**, 715–721.
74. Rubinson, D.A., Dillon, C.P., Kwiatkowski, A.V., Sievers, C., Yang, L., Kopinja, J., Rooney, D.L., Zhang, M., Ihrig, M.M., McManus, M.T. *et al.* (2003) A lentivirus-based system to functionally silence genes in primary mammalian cells, stem cells and transgenic mice by RNA interference. *Nat. Genet.*, **33**, 401–406.
75. Ng, Y., Ramm, G., Lopez, J.A. and James, D.E. (2008) Rapid activation of Akt2 is sufficient to stimulate GLUT4 translocation in 3T3-L1 adipocytes. *Cell Metab.*, **7**, 348–356.
76. Carter, E.A., Rayner, B.S., McLeod, A.I., Wu, L.E., Marshall, C.P., Levina, A., Aitken, J.B., Witting, P.K., Lai, B., Cai, Z. *et al.* (2010) Silicon nitride as a versatile growth substrate for microspectroscopic imaging and mapping of individual cells. *Mol. BioSyst.*, **6**, 1316–1322.
77. Weekley, C.M., Aitken, J.B., Vogt, S., Finney, L.A., Paterson, D.J., de Jonge, M.D., Howard, D.L., Musgrave, I.F. and Harris, H.H. (2011) Uptake, distribution, and speciation of selenoamino acids by human cancer cells: X-ray absorption and fluorescence methods. *Biochemistry*, **50**, 1641–1650.
78. Vogt, S. (2003) MAPS: A set of software tools for analysis and visualization of 3D X-ray fluorescence data sets. *J. Phys. IV France*, **104**, 635–638.
79. Ruiss, R., Jochum, S., Mocikat, R., Hammerschmidt, W. and Zeidler, R. (2011) EBV-gp350 confers B-cell tropism to tailored exosomes and is a neo-antigen in normal and malignant B cells--a new option for the treatment of B-CLL. *PLoS One*, **6**, e25294.

Downloaded from http://hmg.oxfordjournals.org/ at University of New South Wales on October 13, 2014